Available online at www.sciencedirect.com
ScienceDirect
Deep-Sea Research II 54 (2007) 1268–1291
DEEP-SEA RESEARCH PART II
www.elsevier.com/locate/dsr2

Authigenic carbonate formation at hydrocarbon seeps in continental margin sediments: A comparative study

Thomas H. Naehr[a,*], Peter Eichhubl[b], Victoria J. Orphan[c], Martin Hovland[d], Charles K. Paull[e], William Ussler III[e], Thomas D. Lorenson[f], H. Gary Greene[g]

[a]*Department of Physical and Environmental Sciences, Texas A&M University-Corpus Christi, 6300 Ocean Drive, Corpus Christi, TX 78412, USA*
[b]*University of Texas at Austin, Bureau of Economic Geology, University Station, Box X, Austin, TX 78713-8924, USA*
[c]*Division of Geological and Planetary Sciences, California Institute of Technology, Mail Code 100-23, Pasadena, CA 91125, USA*
[d]*Statoil, 4001 Stavanger, Norway*
[e]*Monterey Bay Aquarium Research Institute, 7700 Sandholdt Road, Moss Landing, CA 95039, USA*
[f]*USGS, 345 Middlefield Road, M.S. 999, Menlo Park, CA 94025, USA*
[g]*Moss Landing Marine Laboratories, 8272 Moss Landing Road, Moss Landing, CA 95039, USA*

Accepted 16 April 2007
Available online 20 July 2007

Abstract

Authigenic carbonates from five continental margin locations, the Eel River Basin, Monterey Bay, Santa Barbara Basin, the Sea of Okhotsk, and the North Sea, exhibit a wide range of mineralogical and stable isotopic compositions. These precipitates include aragonite, low- and high-Mg calcite, and dolomite. The carbon isotopic composition of carbonates varies widely, ranging from −60‰ to +26‰, indicating complex carbon sources that include ^{13}C-depleted microbial and thermogenic methane and residual, ^{13}C-enriched, bicarbonate. A similarly large variability of δ^{18}O values (−5.5‰ to +8.9‰) demonstrates the geochemical complexity of these sites, with some samples pointing toward an ^{18}O-enriched oxygen source possibly related to advection of ^{18}O-enriched formation water or to the decomposition of gas hydrate. Samples depleted in ^{18}O are consistent with formation deeper in the sediment or mixing of pore fluids with meteoric water during carbonate precipitation.

A wide range of isotopic and mineralogical variation in authigenic carbonate composition within individual study areas but common trends across multiple geographic areas suggest that these parameters alone are not indicative for certain tectonic or geochemical settings. Rather, the observed variations probably reflect local controls on the flux of carbon and other reduced ions, such as faults, fluid conduits, the presence or absence of gas hydrate in the sediment, and the temporal evolution of the local carbon reservoir.

Areas with seafloor carbonates that indicate formation at greater depth below the sediment–water interface must have undergone uplift and erosion in the past or are still being uplifted. Consequently, the occurrence of carbonate slabs on the seafloor in areas of active hydrocarbon seepage is commonly an indicator of exhumation following carbonate precipitation in the shallow subsurface. Therefore, careful petrographic and geochemical analyses are critical components necessary for the correct interpretation of processes related to hydrocarbon seepage in continental margin environments and elsewhere.

Keyword: Seeps; Methane; Authigenic; Carbonate; Continental margins

*Corresponding author. Tel.: +1 361 825 2470; fax: +1 361 825 2025.
E-mail address: thomas.naehr@tamucc.edu (T.H. Naehr).

0967-0645/$ - see front matter © 2007 Elsevier Ltd. All rights reserved.
doi:10.1016/j.dsr2.2007.04.010

1. Introduction

Hydrocarbon seeps are ubiquitous features of many active and passive continental margins. They represent discrete sites where fluids in chemical disequilibrium with seawater and typically rich in methane and other hydrocarbons travel through the sub-seafloor environment and emanate at the sediment–water interface. Thiotrophic or methanotrophic biological communities and precipitates of authigenic minerals mark such areas of fluid discharge, and are the result of both biogeochemical turnover and the interaction between fluids and ambient bottom water at hydrocarbon seep sites (Hovland et al., 1985; Suess et al., 1985; Paull et al., 1995b; Naehr et al., 2000a, b). Bicarbonate and sulfate activities at hydrocarbon seeps are predominately controlled by the flux of gases, mostly methane, to the seafloor, and by rates of biologically induced reactions. Furthermore, chemosymbiotic benthic fauna is supported by the microbially driven anaerobic oxidation of methane (AOM) (Elvert and Suess, 1999; Hinrichs et al., 1999; Thiel et al., 1999), which increases pore water alkalinity by the production of bicarbonate [HCO_3^-]:

$$CH_4 + SO_4^{2-} \Leftrightarrow HCO_3^- + HS^- + H_2O \quad (1)$$

thus favoring precipitation of authigenic carbonate minerals in the shallow subsurface by the reaction

$$2HCO_3^- + Ca^{2+} \Leftrightarrow CaCO_3 + CO_2 + H_2O \quad (2)$$

(Baker and Burns, 1985).

Authigenic carbonates associated with hydrocarbon seepage are known to show a wide range of mineralogical as well as carbon and oxygen isotopic compositions. The occurrence of high-Mg calcite (HMC) and low-Mg calcite (LMC), aragonite, dolomite, and other less common mineral species, such as glendonite or ikaite, has been documented by various authors (e.g., Claypool and Kaplan, 1974; Greinert et al., 2001; Greinert and Derkachev, 2004; Orphan et al., 2004). The carbon isotopic composition of these carbonates can vary by as much as 85‰, indicating an almost equally wide range of geochemical processes involved in carbonate precipitation. Oxygen isotopes also may show considerable variation, documenting the effects of temperature and/or fluid composition on carbonate formation. Regardless of their mineralogical and isotopic composition, however, seep-related authigenic minerals provide an important geological archive, as they represent one of the few permanent records of an otherwise ephemeral phenomenon (Naehr et al., 2000b; Martin et al., 2004; Hein et al., 2006).

The aim of this paper is to develop a more comprehensive understanding of the complex geochemical, physical, and biological interactions at seep sites by comparing the mineralogy, petrology, and isotope geochemistry of authigenic carbonates from five different hydrocarbon seep locations. In doing so, we hope to address the question whether the biogeochemistry of hydrocarbon seeps varies systematically between different locations or if the observed geochemical trends reflect local controls on the flux of carbon from the subsurface to the seafloor. To this end, we present a comparative study that illustrates the diverse processes associated with the flux of fluids and gases to the seafloor and the precipitation of authigenic minerals at hydrocarbon seeps. We shall discuss and contrast the formation and early diagenesis of authigenic mineral deposits in a variety of geologic and geochemical environments including Eel River Basin, Monterey Bay, Santa Barbara Basin, the Sea of Okhotsk, and the North Sea (Fig. 1).

2. Geologic setting

The Eel River Basin is a forearc basin located at the southern end of the Cascadia accretionary prism that is associated with the Gorda-North American plate margin (Fig. 1A). The dominant structural features that define the Eel River Basin include a series of NNW–SSE trending synclines, anticlines, and faults that form a 250-km-long and 70-km-wide sedimentary basin (Hoskins and Griffiths, 1971; Carver, 1987; Clarke, 1992). The Eel River Basin is underlain by Jurassic to Eocene rocks of the Franciscan Complex and contains a 4000-m thick sequence of Neogene age sediments that primarily consist of marine mudstones, siltstones, and fine sandstones (Carver, 1987; Clarke, 1992). Because the organic carbon content and thickness of these sediments are adequate to generate petroleum, the basin has been a recurring target for hydrocarbon exploration. Gas production still occurs from the Tomkins Hill Gas Field and small amounts of oil were produced from onshore basins (McCulloch et al., 1977; Horan and Hopps, 1987). Modern sedimentation in the Eel River Basin is controlled by sediment input from the Eel and Mad rivers, with the vast majority of sediment being transported during short-duration storm events (Orange,

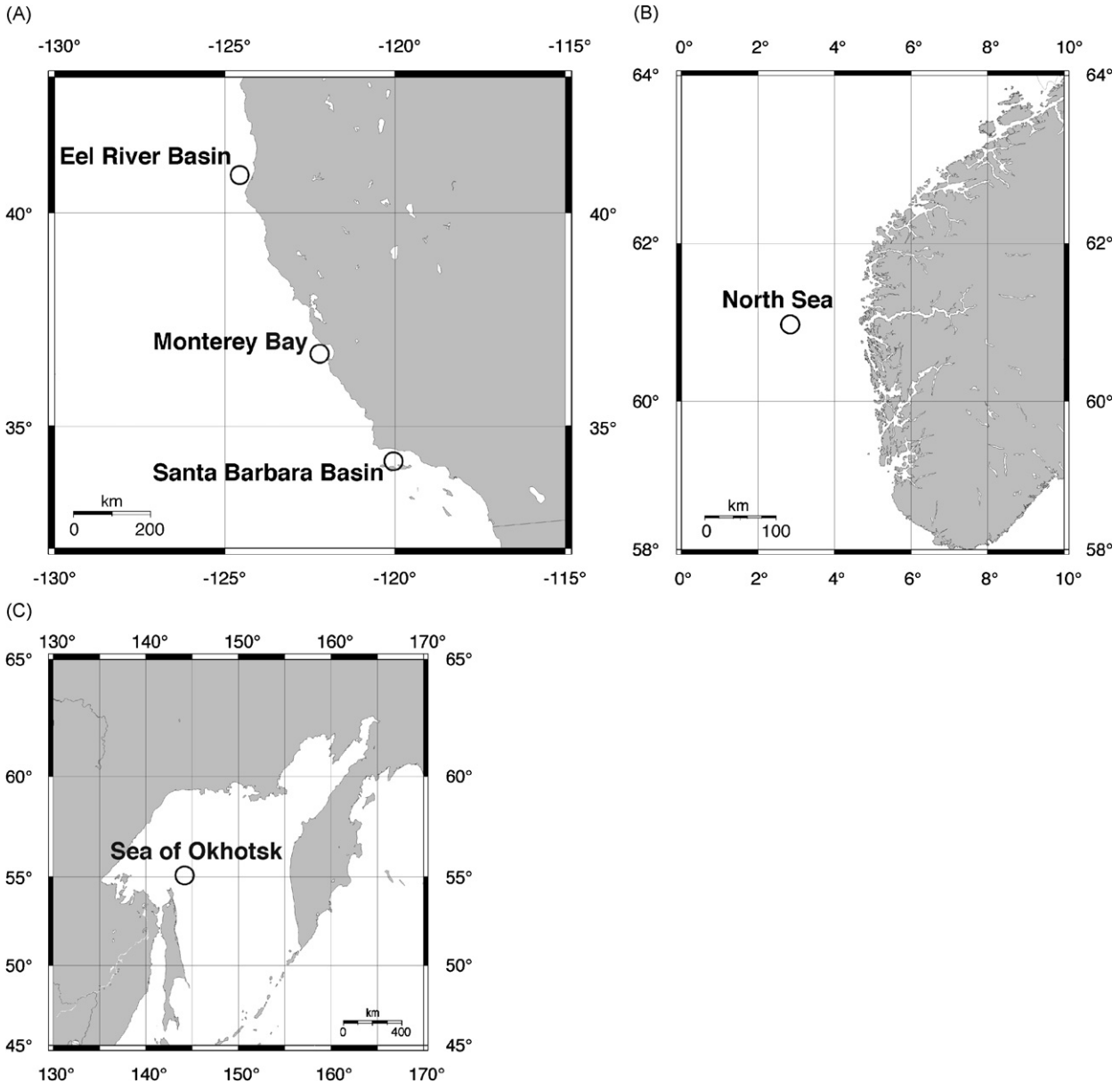

Fig. 1. Location maps of the study areas. (A) Location of Eel River Basin, Monterey Bay, and Santa Barbara Basin along the western continental margin of the North American plate. (B) Location of the Tommeliten study area in the central North Sea. (C) Location map of samples from the western flank of the Derugin Basin in the Sea of Okhotsk.

1999). Secondary transport of sediment by mass wasting and sediment redistribution also plays an important role in this tectonically active environment. Rapid tectonic uplift and high erosion rates are responsible for high sediment-accumulation rates in the Eel River Basin (Alexander et al., 1999). Furthermore, the basin receives large quantities of young, relatively fresh organic matter during floods of the Eel and other rivers (Leithold et al., 1999).

Monterey Bay and its deep canyon rest on the active transform boundary that separates the Pacific plate from the North American plate (Fig. 1A). In central California, this boundary is more than 100 km wide and includes the San Andreas fault to the east, as well as offshore segments of the Palo

Colorado–San Gregorio fault and Monterey Bay fault zone to the west. These fault zones are seismically active and in many places offset the seafloor or Quaternary sedimentary rocks. The western margin of California also has been influenced by northeast–southwest-directed compression (Mount and Suppe, 1992) that has produced thrust faults, folds, and localized uplift west of the San Gregorio fault zone in the Monterey Bay region, an area previously referred to as Smooth Ridge (Greene, 1990; Orange et al., 1999). A number of both extinct and active hydrocarbon seeps have previously been described in this area (e.g., Barry et al., 1996; Martin et al., 1997; Orange et al., 1999; Stakes et al., 1999; Aiello, 2005). Active sites are associated with live chemosynthesis-based communities fueled by the expulsion of sulfide and/or methane-rich fluids. Authigenic carbonate precipitates delineate both active and extinct seep sites. The sedimentary sequence in the Monterey Bay region consists of as much as 2.4 km of Tertiary and Quaternary sedimentary strata that unconformably overlie Cretaceous granitic basement rocks (Greene, 1977). In the Smooth Ridge area, the oldest sedimentary units of this sequence include 0–640 m of the Monterey Formation, a petroliferous, siliceous mudstone sequence of Miocene age. The Monterey Formation is either exposed on the seafloor or unconformably overlain by the Purisima Formation, an up to 210-m thick sequence of nearshore marine sandstone of Late Miocene to Pliocene age (Greene, 1977).

The *Santa Barbara Basin*, part of the continental borderland of southern California (Fig. 1A), is composed of a Cretaceous to Holocene sequence of clastic and hemipelagic units. The sedimentary sequence includes organic-rich siliceous mudstone of the Miocene Monterey Formation that is both source and fractured reservoir of hydrocarbons. While the northern flanks of the basin are being actively folded and exhumed as part of the Santa Ynez Mountains, the central part of the basin is undergoing sedimentation and prograde burial. Transpressive shortening of the basin flanks is accommodated by high-angle oblique reverse and strike-slip faults and by folds with faulted anticlines. Prograde burial and diagenesis in synclines and in the basin center drive hydrocarbon generation and pore fluid expulsion, leading to submarine seepage of natural gas and oil (Vernon and Slater, 1963; Allen et al., 1970; Wilkinson, 1971). Due to the low matrix permeability of the siliceous mudstone, fluid flow within and out of the Monterey Formation depends on the presence of conductive fracture and fault systems. Evidence of focused fluid flow along faults is seen in surface outcrops and core samples across faults that are extensively cemented with carbonate (Eichhubl and Behl, 1998). Based on mass balance estimates of fluid involved in fault cementation, Eichhubl and Boles (2000) inferred that faults channel fluid migrating up along the tilted flanks of the basin, providing cross-stratigraphic pathways for fluid expulsion to higher structural levels and to the surface.

The *Tommeliten* study area in the central North Sea (Block 1/9; Fig. 1B) is located above a buried salt diapir, the so-called Delta structure in a water depth of about 74 m (Hovland, 2002). The top of the salt diapir lies about 1 km below the seafloor, and is covered by horizontally stratified Mesozoic and Quaternary sandy and clay-rich sediments. Above this structure is a large acoustically disturbed zone, indicating extensive gas charging of subsurface sediments (D'Heur et al., 1987; Hovland et al., 1993). Gas escapes to the seabed along deep-seated faults, and evidence of gas identified by acoustic turbidity close to the seabed is present over an area of approximately 120,000 m^2 (Hovland and Sommerville, 1985; Niemann et al., 2005).

The *Sea of Okhotsk* is part of the western Pacific Ocean, located between the Kamchatka Peninsula and the Kurile Islands to the east, the Japanese island of Hokkaido to the south, and the island of Sakhalin to the west (Fig. 1C). The main bathymetric feature is the Derugin Basin with water depths of up to 1800 m. The western flank of the basin coincides with the eastern slope of Sakhalin Island, from where the samples described in this study were recovered (Ginsburg et al., 1993). The basin is filled with up to 6 km of Eocene through Quaternary sediments rich in diatoms and radiolarians, reflecting the high primary productivity of the Sea of Okhotsk (Greinert et al., 2002). Authigenic carbonate and massive barite deposits are known from the Derugin Basin and have been described by various authors (Astakhova, 1997; Lorenson et al., 1999; Greinert et al., 2002). Tectonic features of the basin include horst and graben structures, caused by NW–SE directed strike-slip faulting and NE–SW trending thrust and normal faults that may act as migration pathways for ascending fluids (Greinert et al., 2002).

3. Methods

3.1. Seafloor observations and sampling

Samples described in this study were collected using remotely operated vehicles (ROVs). The purpose of these dives was the investigation of fluid-flow- and gas-expulsion-related seafloor features as well as the search for gas hydrate occurrences in continental margin sediments. Our exploration efforts usually focused on areas where dive targets were associated with high seafloor reflectivity and enhanced topographic relief in high-resolution multibeam bathymetric and reflectivity data. For example, exploration in the Eel River Basin focused on a region near the crest of a broad NNW–SSE trending anticlinal structure with high seafloor reflectivity and enhanced local relief (Orphan et al., 2004). Irregularly shaped pieces of authigenic carbonate crusts and slabs are prominent seafloor features in all areas described in this study, frequently forming extensive pavements adjacent to chemosynthesis-based biological communities and sites of active fluid or gas seepage. Commonly, erosion has exposed multiply stacked authigenic carbonate slabs, indicating several phases of carbonate precipitation. Sampling efforts in these locations usually encounter hard substrate or firm sediment within 10–20 cmbsf (centimeters below seafloor) and authigenic carbonate nodules can commonly be observed within the deeper intervals of cored samples. These observations suggest that in areas of active fluid seepage large portions of the seafloor may be underlain by extensive layers of authigenic carbonates.

Samples of seafloor carbonate slabs were collected using the ROV's manipulator arms, described, photographed, and subsequently stored at room temperature for sectioning, subsampling, and analysis. In addition, seafloor sediment, megafauna, and microbiological samples were obtained using ROV-collected push cores and hydraulic piston cores. Sediment cores were described, extruded, and sampled for pore water geochemistry, percent water content, carbonates, lipid biomarkers, molecular and microscopy analyses, and anaerobic cultivation. Results of these analyses were described elsewhere (Eichhubl et al., 2000; Naehr et al., 2000b; Orphan et al., 2004).

3.2. Carbonate mineralogy and petrography

Bulk mineralogy and the relative abundance of carbonate minerals in each sample were determined by X-ray diffraction using a Philips PW 1820 X-ray diffractometer at the Leibniz Institute of Marine Sciences at the University of Kiel (IFM-GEOMAR), and a Rigaku Ultima III X-ray diffractometer at Texas A&M University-Corpus Christi. Samples for XRD analyses were prepared following standard procedures using an internal corundum standard (Naehr et al., 2000a). Scans were run from 2° to 60° 2θ at a scanning speed of 0.01° 2θ/s. The relative proportions of different carbonate minerals were quantified on the basis of the (1 0 4) peak areas of calcite, Mg-calcite and dolomite, and the (1 1 1) peak area of aragonite using calibration curves after Greinert et al. (2001). The position of the (1 0 4) peak was used to determine the Mg content of carbonate minerals (Goldsmith et al., 1961; Lumsden, 1979). For the purpose of this study, calcite with less than 5 mol% $MgCO_3$ is considered LMC and calcite compositions of 5–20 mol% $MgCO_3$ are referred to as HMC after Burton and Walter (1991). Carbonate phases with 30–40 mol% $MgCO_3$ were classified as protodolomite, and carbonates containing 40–55 mol% $MgCO_3$ are referred to as dolomite. Carbonate content (expressed as weight percent (wt%) $CaCO_3$) of the samples was determined using a coulometer at Stanford University, CA. Textural, compositional, and morphological features of carbonate precipitates were studied on hand specimens, slabs, and polished thin sections using light microscopy.

3.3. Carbonate and pore water stable isotope analyses

Samples for oxygen and carbon isotope analyses were obtained from the surfaces of polished slabs using a hand-held microdrill. Stable isotopes of carbon and oxygen were measured at the Stable Isotope Laboratory, University of California Santa Cruz (UCSC), and the Stanford University Stable Isotope Laboratory. The CO_2 for analysis was obtained by reacting samples with 100% orthophosphoric acid in vacuo at 70 (Stanford) and 90 °C (UCSC), respectively. The purified CO_2 gas was analyzed using standard mass spectrometric techniques. Results are reported in standard δ notation relative to the PDB standard. Precision is on the order of 0.03‰ for both oxygen and carbon. Because of the unequal oxygen isotope fractionation during CO_2 generation using H_3PO_4, dolomite $\delta^{18}O$ values have an analytical offset compared to calcite of $+1.33$‰ at 90 °C and $+1.54$‰ at 70 °C reaction

temperature (Rosenbaum and Sheppard, 1986; Swart et al., 1991). Our data are corrected for this offset when used to calculate temperatures of dolomite precipitation or pore water oxygen isotopic compositions. Our calculations of equilibrium formation temperatures or pore water isotopic compositions are based on equations by Friedman and O'Neil (1977) for Mg-calcite, Hudson and Anderson (1989) for aragonite, and Irwin (1980) for protodolomite and dolomite. Carbon isotopic analyses of pore water methane and carbon dioxide were carried out at the Department of Marine Sciences, University of North Carolina, Chapel Hill, NC, using a GC-IRMS (Finnigan MAT-252) and are reported in standard δ notation relative to the PDB standard.

3.4. Strontium isotope analysis

The $^{87}Sr/^{86}Sr$ composition of 14 carbonate samples was determined using a VG-Sector 54 thermal ionization mass spectrometer at the Department of Geology, University of North Carolina at Chapel Hill. Samples for $^{87}Sr/^{86}Sr$ analysis were microdrilled adjacent to samples for $\delta^{13}C$ and $\delta^{18}O$ determination. Samples were dissolved in 500 μL 1 M ultra-pure acetic acid, centrifuged, and the decantate was evaporated dry. Samples were then redissolved in 250 μL of 5 N HNO_3, and loaded into columns containing Eichrom Sr-specific resin. Details of the procedure are described in Paull et al. (1995a). Values of $^{87}Sr/^{86}Sr$ are reported relative to a $^{87}Sr/^{86}Sr$ ratio of 0.71025 for SRM-987. Replicate analyses of SRM indicate uncertainties of ± 0.000011 (1σ).

4. Results

4.1. Mineralogy and petrographic description

Carbonate mineralogies are summarized in Table 1 and Fig. 2. Carbonate contents of the carbonate crusts from the Eel River Basin vary between 27% and 87% $CaCO_3$, with a mean of 63% (Table 1). These values are significantly higher than the $CaCO_3$ values of the unconsolidated near-surface sediments in the area, which range from $<1\%$ to 17% with an average of 3.6% (Orphan et al., 2004). Carbonate mineralogy in the Eel River Basin (Fig. 2A) is characterized by the occurrence of HMC (average 15 mol% $MgCO_3$), aragonite, and dolomite (46–50 mol% $MgCO_3$). HMC is the most common authigenic carbonate in Eel River Basin samples, often forming a primary cement within sediment intraclasts (Fig. 3A). Frequently, micritic HMC cements the pore space between individual sediment components, followed by sparitic aragonite filling voids and cracks between intraclasts (Figs. 3B and C). Dolomite, on the other hand, does not coexist with either Mg-calcite or aragonite, but forms the microcrystalline matrix of carbonate-cemented sand-, silt-, and mudstones (Fig. 3D).

Authigenic carbonates from the Santa Barbara Basin are typically composed of HMC, aragonite, and dolomite in varying proportions (Fig. 2B), cementing the silty and locally sandy to pebbly sediment. Aragonite occurs both as a microcrystalline cement and as layered, acicular botryoids that fill the pore space between sediment grains. Dolomite tends to form isopachous cements in the coarser-grained sediments (Eichhubl et al., 2000).

The seafloor carbonates from Monterey Bay are typically carbonate-cemented sand-, silt-, or mudstones with carbonate contents between 40 and 90 wt% $CaCO_3$ (Fig. 2C). Subhedral, pore-filling micrite followed by botryoidal to sparitic aragonite are the dominant cement types (Fig. 3E). Samples from the location Portuguese Ledge are coarse-grained sandstones and conglomerates that are cemented by poikilotopic micritic to sparitic LMC cements. Cabrillo Canyon Head samples are brecciated silty mudstones with micritic pore-filling HMC cements and botryoidal aragonite that fills late extension cracks and commonly displays a rhythmic layering. Pyrite framboids are common (Fig. 3F). Similar carbonates occur at Chimney Field in addition to dolomite-cemented mudstones and silty mudstones with microcrystalline mixtures of dolomite and HMC. Aragonite is absent from Clamfield and Horse Shoe Scarp samples, which are dominated by siltstones and silty claystones that are cemented by micritic HMC and dolomite. Carbonate-cemented rocks from Greene Wall are very coarse-grained sandstones cemented by micritic HMC (sample 1074-RS1) or conglomerates with isopachous rim cements consisting of protodolomite (sample 1074-RS2).

Seafloor carbonates from the North Sea are silty mudstones with pore-filling carbonate cements consisting mostly of microcrystalline aragonite with subordinate amounts of LMC (Figs. 2D, 3G, and H). Micritic HMC is the dominant cement in the silty mudstones from the Sea of Okhotsk (Fig. 2E). Aragonite was found in only two samples as pore-filling microcrystalline cement.

Table 1
Mineralogical and stable isotopic composition of samples from hydrocarbon seep areas

Sample	Qtz (%)	LMC (%)	mol% Mg	HMC (%)	mol% Mg	Arag. (%)	Protodol./ dolo. (%)	mol% Mg	$\delta^{18}O$ (‰)	$\delta^{13}O$ (‰)	Probable geochemical environment
Monterey Bay											
Cabrillo Canyon Head											
738-RS4 aragonite	–	–	–	–	–	100	–	–	4.80	−47.61	Active seepage
738-RS4 fractured	18	–	–	100	13	–	–	–	5.73	−53.26	Active seepage
Portuguese Ledge											
PL-1	28	100	2	–	–	–	–	–	−5.52	−11.04	Meteoric water?
992-RS2	22	100	2	–	–	–	–	–	−5.38	−10.89	Meteoric water?
1015-RS1	24	100	2	–	–	–	–	–	−5.51	−10.81	Meteoric water?
Chimney Field											
1030-RS1	8	–	–	–	–	–	100	46	5.77	−44.19	Active seepage
1030-RS2	14	–	–	100	10	–	–	–	5.17	−47.65	Active seepage
1030-RS6	15	–	–	54	19	–	46	42	6.37	−42.99	Active seepage
1030-RS7	14	–	–	100	14	–	–	–	4.52	−50.09	Active seepage
1088-RS1	13	–	–	100	13	–	–	–	5.38	−55.61	Active seepage
1088-RS2A aragonite	–	–	–	–	–	100	–	–	4.66	−48.28	Active seepage
1088-RS2A fractured	16	–	–	100	14	–	–	–	6.08	−47.07	Active seepage
1088-RS2A homogenous	17	–	–	100	11	–	–	–	5.75	−48.82	Active seepage
1088-RS2B	12	–	–	–	–	–	100	46	5.73	−35.69	Active seepage
1093-RS1B	14	–	–	–	–	–	100	45	5.58	−39.74	Active seepage
1093-RS2B	21	–	–	–	–	–	100	45	5.78	−38.30	Active seepage
Clamfield											
1364-RS1	7	–	–	100	8	–	–	–	5.36	−23.56	Active seepage
1364-RS2	8	–	–	100	9	–	–	–	5.52	−18.24	Active seepage
Greene Wall											
1074-RS1A	11	–	–	100	6	–	–	–	–2.40	−25.32	Active seepage
1074-RS2	21	–	–	–	–	–	100	40	4.61	−54.04	Active seepage
Horse Shoe Scarp											
1053-RS2	15	–	–	100	10	–	–	–	–2.00	−46.90	Active seepage
1053-RS3	8	–	–	100	13	–	–	–	4.61	−40.00	Active seepage
1062-RS1	12	–	–	76	8	–	24	35	3.46	0.17	Low flux
1062-RS2	4	–	–	–	–	–	100	46	4.77	−5.15	Low flux
1062-RS3	11	–	–	68	8	–	32	36	4.94	−50.50	Active seepage
1062-RS4	10	–	–	–	–	–	100	46	5.24	−20.30	Active seepage
1363-RS1	9	–	–	97	11	–	3	35	5.03	−33.60	Active seepage
1363-RS2	5	–	–	–	–	–	100	50	3.58	9.10	Methanogenesis

Eel River Basin											
Little Salmon Fault											
1294-RS-2a	n.d.	–	–	–	–	–	100	44	6.35	9.30	Methanogenesis
1294-RS-2b	n.d.	–	–	–	–	–	100	44	6.41	8.68	Methanogenesis
1297-RS-1	n.d.	57	n.d.	–	–	–	43	31	5.32	−26.04	Active seepage
1297-RS-2	n.d.	–	–	–	–	–	100	49	6.52	6.10	Methanogenesis
1297-RS-3	n.d.	–	–	80	8	–	20	35	5.14	−15.48	Active seepage
1303-RS-1	n.d.	–	–	66	9	–	34	35	4.01	−30.00	Active seepage
1303-RS-2	n.d.	–	–	100	16	–	–	–	5.16	−23.70	Active seepage
1303-RS-3	n.d.	–	–	72	11	–	28	35	5.24	−26.53	Active seepage
1303-RS-4	n.d.	–	–	100	16	–	–	–	5.21	−37.82	Active seepage
1303-RS-5	n.d.	–	–	100	18	–	–	–	5.00	−23.64	Active seepage
1303-RS-6	n.d.	–	–	100	16	–	–	–	4.49	−18.97	Active seepage
1303–PC-26	n.d.	–	–	100	9	–	–	–	4.43	−24.13	Active seepage
1307-RS-1a	n.d.	5	n.d.	95	18	–	–	–	5.13	−15.41	Active seepage
1307-RS-1b	n.d.	–	–	–	–	100	–	–	3.93	−27.59	Active seepage
1307-RS-1c	n.d.	–	–	100	17	–	–	–	5.16	−11.70	Active seepage
1307-RS-1d	n.d.	–	–	–	–	99	–	–	3.61	−25.77	Active seepage
1307-HPC-1	n.d.	–	–	100	16	–	–	–	4.35	−40.03	Active seepage
1307-HPC-4	n.d.	–	–	92	10	–	8	34	4.73	−26.17	Active seepage
Table Bluff Anticline											
1657-RS2	9	–	–	–	–	100	–	–	4.73	−27.35	Active seepage
1657-RS3	8	–	–	–	–	–	100	48	8.13	5.57	Methanogenesis
1658-RS1	5	–	–	–	–	–	100	49	8.88	7.97	Methanogenesis
1658-RS2	10	–	–	5	16	95	–	–	3.95	−37.13	Active seepage
1658-RS4	4	–	–	–	–	–	100	53	8.30	15.09	Methanogenesis
1658-RS7	5	–	–	–	–	–	100	50	8.08	5.02	Methanogenesis
1658-RS8	22	–	–	–	–	100	–	–	3.43	−36.11	Active seepage
1659-RS1	–	–	–	–	–	100	–	–	4.14	−38.41	Active seepage
1659-RS1 rep1	–	–	–	–	–	100	–	–	4.20	−38.73	Active seepage
1659-RS1 rep2	–	–	–	–	–	100	–	–	3.80	−33.06	Active seepage
1659-RS4	13	–	–	100	17	–	–	–	4.17	−31.02	Active seepage
1660-RS1	12	–	–	2	16	98	–	–	4.77	−35.84	Active seepage
1660-RS2	11	–	–	–	–	–	100	46	6.73	6.76	Methanogenesis
1663-RS1	6	–	–	–	–	–	100	51	7.70	8.03	Methanogenesis
1664 box core top	8	–	–	100	17	–	–	–	4.50	−36.01	Active seepage
1664 box core bottom	8	–	–	100	16	–	–	–	4.53	−37.24	Active seepage
1664 clathr. bucket	10	–	–	100	16	–	–	–	4.43	−33.94	Active seepage
1664-RS2	7	–	–	–	–	–	100	50	8.17	13.13	Methanogenesis
ER-82											
1298	n.d.	–	–	–	–	99	–	–	3.19	−31.44	Active seepage
1298-RS-1	n.d.	–	–	100	15	–	–	–	4.12	−33.07	Active seepage
1298-RS-2a	n.d.	–	–	62	9	–	38	39	5.65	−22.08	Active seepage
1298-RS-2b	n.d.	–	–	60	9	–	40	36	5.63	−22.22	Active seepage
1298-RS-3	n.d.	–	–	67	8	–	33	35	5.52	−22.68	Active seepage

Table 1 (*continued*)

Sample	Qtz (%)	LMC (%)	mol% Mg	HMC (%)	mol% Mg	Arag. (%)	Protodol./ dolo. (%)	mol% Mg	$\delta^{18}O$ (‰)	$\delta^{13}O$ (‰)	Probable geochemical environment
1300-HPC-5 top	n.d.	–	–	100	14	–	–	–	5.38	−33.64	Active seepage
1300-HPC-5 base	n.d.	–	–	100	16	–	–	–	3.98	−29.22	Active seepage
1306-RS-1	n.d.	–	–	79	7	–	21	31	5.39	−25.43	Active seepage
1306-RS-2	n.d.	–	–	100	14	–	–	–	5.84	−31.31	Active seepage
1661-PC-22 2–9 cm	11	–	–	100	19	–	–	–	4.58	−36.99	Active seepage
Santa Barbara Basin											
1490-1	3	–	–	–	–	–	100	n.d.	5.22	24.90	Methanogenesis
1490-3	4	–	–	–	–	–	100	n.d.	5.18	21.25	Methanogenesis
1490-4	3	–	–	–	–	–	100	n.d.	0.35	13.46	Methanogenesis
1490-5	2	–	–	–	–	–	100	n.d.	6.24	9.63	Methanogenesis
1490-7	6	–	–	–	–	–	100	n.d.	3.03	11.14	Methanogenesis
1492-1B-cc	17	38	n.d.	–	–	–	62	n.d.	1.18	−27.68	Active seepage
1492-1B-do									3.89	−15.36	Active seepage
1495-1-cc	13	–	–	17	n.d.	58	24	n.d.	4.94	−36.81	Active seepage
1495-1-do									4.77	−5.87	Low flux
1495-3	13	–	–	3	n.d.	97	–	–	2.85	−48.64	Active seepage
1495-4	5	–	–	38	n.d.	61	–	–	3.75	−51.32	Active seepage
1499-2	12	–	–	41	n.d.	59	–	–	3.77	−31.05	Active seepage
1501-1	2	9	–	28	n.d.	–	63	n.d.	5.70	8.59	Methanogenesis
1501-2A	29	100	n.d.	–	–	–	–	–	–5.36	−13.27	Active seepage
1502-1	1	–	–	–	–	–	100	n.d.	7.32	26.31	Methanogenesis
1503-1-hmc	16	–	–	43	n.d.	–	57	n.d.	5.13	−16.32	Active seepage
1503-1-do									4.09	−5.33	Low flux
1503-2	11	–	–	3	n.d.	97	–	–	4.02	−57.50	Active seepage
1504-1	3	–	–	–	–	–	100	n.d.	4.39	13.03	Methanogenesis
1507-1-cc	11	38	n.d.	–	–	–	62	n.d.	5.37	−8.63	Low flux
1507-1-do									5.00	−10.41	Active seepage
1507-4	4	–	–	100	n.d.	–	–	–	6.59	−25.97	Active seepage
148-1	9	–	–	41	n.d.	–	59	n.d.	3.88	−33.46	Active seepage
148-3	11	–	–	29	n.d.	–	71	n.d.	4.06	−37.30	Active seepage
148-4	13	–	–	29	n.d.	–	71	n.d.	3.98	−39.72	Active seepage
148-6	20	–	–	76	n.d.	–	24	n.d.	4.24	−59.61	Active seepage
149-1	22	–	–	78	n.d.	–	22	n.d.	4.84	−53.79	Active seepage
149-2	10	–	–	–	–	–	100	n.d.	4.47	−44.35	Active seepage
149-3	12	5	n.d.	12	n.d.	–	84	n.d.	4.68	−36.74	Active seepage
149-4a	15	11	n.d.	29	n.d.	–	60	n.d.	4.83	−36.42	Active seepage
149-5	18	30	n.d.	62	n.d.	–	8	n.d.	4.76	−30.25	Active seepage
149-6	23	17	n.d.	57	n.d.	–	26	n.d.	4.37	−59.07	Active seepage
150-1	18	–	–	32	n.d.	–	68	n.d.	3.91	−51.85	Active seepage
150-2	18	3	n.d.	10	n.d.	–	87	n.d.	4.20	−52.56	Active seepage

150-3	11	–	–	8	n.d.	–	92	n.d.	4.60	−38.74	Active seepage
150-4	11	–	–	72	n.d.	–	28	n.d.	4.77	−55.81	Active seepage
150-5	13	–	–	70	n.d.	–	30	n.d.	4.57	−49.55	Active seepage
150-6	12	–	–	4	n.d.	–	96	n.d.	4.75	−15.86	Active seepage
151-1	19	–	–	5	n.d.	–	95	n.d.	4.65	−28.28	Active seepage
151-2	13	4	n.d.	11	n.d.	–	85	n.d.	3.76	−37.13	Active seepage
151-3									4.78	−36.31	Active seepage
151-4	13	–	–	–	–	–	100	n.d.	4.08	−30.18	Active seepage
151-5	15	–	–	19	n.d.	–	81	n.d.	3.56	−26.85	Active seepage
151-6	18	–	–	–	–	99	1	n.d.	3.52	−47.05	Active seepage
151-7	11	–	–	96	n.d.	–	4	n.d.	3.60	−45.86	Active seepage
151-8	9	–	–	50	n.d.	–	50	n.d.	4.18	−35.99	Active seepage
156-1	13	5	–	–	–	–	96	n.d.	4.56	−9.34	Low flux
156-2	11	–	–	5	n.d.	–	95	n.d.	5.05	−16.51	Active seepage
156-4	14	–	–	23	n.d.	74	3	n.d.	4.95	−50.59	Active seepage
156-5	10	–	–	3	n.d.	97	–	–	4.39	−52.14	Active seepage
157-1	13	–	–	38	n.d.	–	62	n.d.	4.19	−19.76	Active seepage
North Sea											
GFC (PM 204)	37	–	–	–	–	100	–	–	3.67	−53.80	Active seepage
GFA 85	26	9	1	–	–	81	10	43	3.79	−41.70	Active seepage
GFA 85 rep.	26	9	1	–	–	81	10	43	3.86	−35.80	Active seepage
TOM 98	45	–	–	–	–	100	–	–	3.83	−34.90	Active seepage
Sea of Okhotsk											
91-02-39	n.d.	–	–	–	–	100	–	–	3.49	−41.72	Active seepage
91-02-51	n.d.	–	–	77	14	23	–	–	3.90	−43.96	Active seepage
91-02-51 burrow	n.d.	–	–	100	12	–	–	–	3.87	−45.73	Active seepage
91-02-54	n.d.	–	–	100	10	–	–	–	3.62	−36.60	Active seepage
91-02-56	n.d.	–	–	100	5	–	–	–	3.46	−27.62	Active seepage
91-02-69	n.d.	–	–	100	6	–	–	–	3.59	−25.84	Active seepage

4.2. Carbon and oxygen isotope data

The $\delta^{13}C$ values of HMC and aragonite within 45 carbonate crust samples from the Eel River Basin (Fig. 4A, groups A and B) vary between −3.2‰ to −40.0‰, with $\delta^{18}O$ values ranging from 3.2‰ to 5.8‰. The $\delta^{13}C$ values of HMC in samples from group B span a wider range than those measured for aragonite (group A). The carbon and oxygen isotope values for the dolomite samples form a distinct group (Fig. 4A, group C), ranging from 5.0‰ to 15.1‰, and from 6.3‰ to 8.9‰, respectively. Carbon isotopic values for methane and carbon dioxide gas extracted from pore water samples (Fig. 5) vary from −27.2‰ to −69.9‰ (CH_4), and from −20.6‰ to −34.0‰ (CO_2).

In Monterey Bay, carbon and oxygen isotopic values vary widely (Fig. 4B). The $\delta^{13}C$ and $\delta^{18}O$ values of authigenic carbonates from six seep sites (Horse Shoe Scarp, Greene Wall, Portuguese Ledge, Clamfield, Cabrillo Canyon Head, Chimney Field) range from −55.6‰ to +9.1‰ and −5.5‰ to +6.4‰, respectively. Fig. 4B shows the data in comparison with five distinct groups for Monterey Bay seep carbonates after Stakes et al. (1999).

Santa Barbara basin samples show carbon and oxygen isotopic variations even greater than the samples from Monterey Bay. The carbon isotopic values vary from −57.5‰ to +26.3‰, with a range of oxygen isotopes from 1.2‰ to 7.3‰. With $\delta^{13}C$ values of +10‰ to +25‰, samples 1490-1–1490-7 contain some of the highest carbon isotopic ratios observed in this study (Fig. 4C). These values were obtained from apparently reworked, rounded dolostones that are texturally and isotopically identical with dolostones of the Miocene Monterey Formation. Stable isotope data for samples from the North Sea and Sea of Okhotsk are shown in Fig. 4D. The $\delta^{13}C$ values for the North Sea samples vary between −34.9‰ and −53.8‰ with a narrow range of $\delta^{18}O$ values from 3.7‰ to 3.8‰. Six authigenic carbonate samples from the Sea of Okhotsk display $\delta^{13}C$ and $\delta^{18}O$ values ranging from −25.8‰ to −45.73‰ and 3.5‰ to 3.9‰, respectively.

4.3. Sr-isotope data

$^{87}Sr/^{86}Sr$ ratios of 14 samples from the Eel River Basin range between 0.708682 and 0.709211 (Fig. 6). Within this sample set, aragonitic samples typically display more radiogenic values (i.e., higher $^{87}Sr/^{86}Sr$ ratios), with values close to modern seawater (0.709175), whereas dolomite-cemented mudstones are characterized by less radiogenic strontium values. HMC samples generally plot in between these two extremes. A comparison of these data with an Sr curve for modern through Miocene seawater (Paytan et al., 1993) shows that authigenic carbonates with $^{87}Sr/^{86}Sr$ values that are less radiogenic then modern seawater must have formed either at or near the seafloor during the Neogene or in contact with less radiogenic pore fluids, presumably deeper in the sediment. Strontium isotope analyses on authigenic carbonates from the North Sea revealed $^{87}Sr/^{86}Sr$ values between 0.709157 and 0.709184, indicating carbonate formation from water with Sr values similar to modern seawater.

5. Discussion

Authigenic carbonate precipitation at hydrocarbon seeps will only take place when pore fluids become sufficiently supersaturated with respect to a carbonate phase and crystallization is not inhibited by kinetic factors (Burton, 1993). Because of the low solubility of carbonate mineral phases in aqueous solutions, many thousand times the pore volume of fluid must pass through the sediment in order to cement the pore space (Luff et al., 2004). Whereas the AOM is responsible for carbonate formation in the shallow subsurface, carbonate precipitation deeper in the sedimentary section may be associated with methane production (Orphan et al., 2004), gas hydrate formation (Kastner et al., 1990), or decomposition (Matsumoto, 1989). Accordingly, authigenic carbonates may show a wide spread of carbon isotopic compositions, ranging from ^{13}C-depleted samples with $\delta^{13}C$ values as low as –60‰ produced by the anaerobic oxidation of isotopically light methane to ^{13}C-enriched samples with $\delta^{13}C$ values of up to +30‰ that represent carbonate precipitation due to methanogenesis deeper in the sediment column (e.g., Claypool and Kaplan, 1974; Naehr et al., 2000a; Greinert et al., 2001; Orphan et al., 2004; Gieskes et al., 2005). In any case, however, the resulting carbonate minerals will reflect the isotopic signature of the total dissolved CO_2 (DIC) pool at the time of carbonate precipitation. Oxygen isotopic values also may vary considerably, with some carbonate samples pointing toward a heavy, ^{18}O-enriched oxygen source, possibly related to dissolution of early diagenetic minerals or the decomposition of gas hydrate (isotopic fractionation

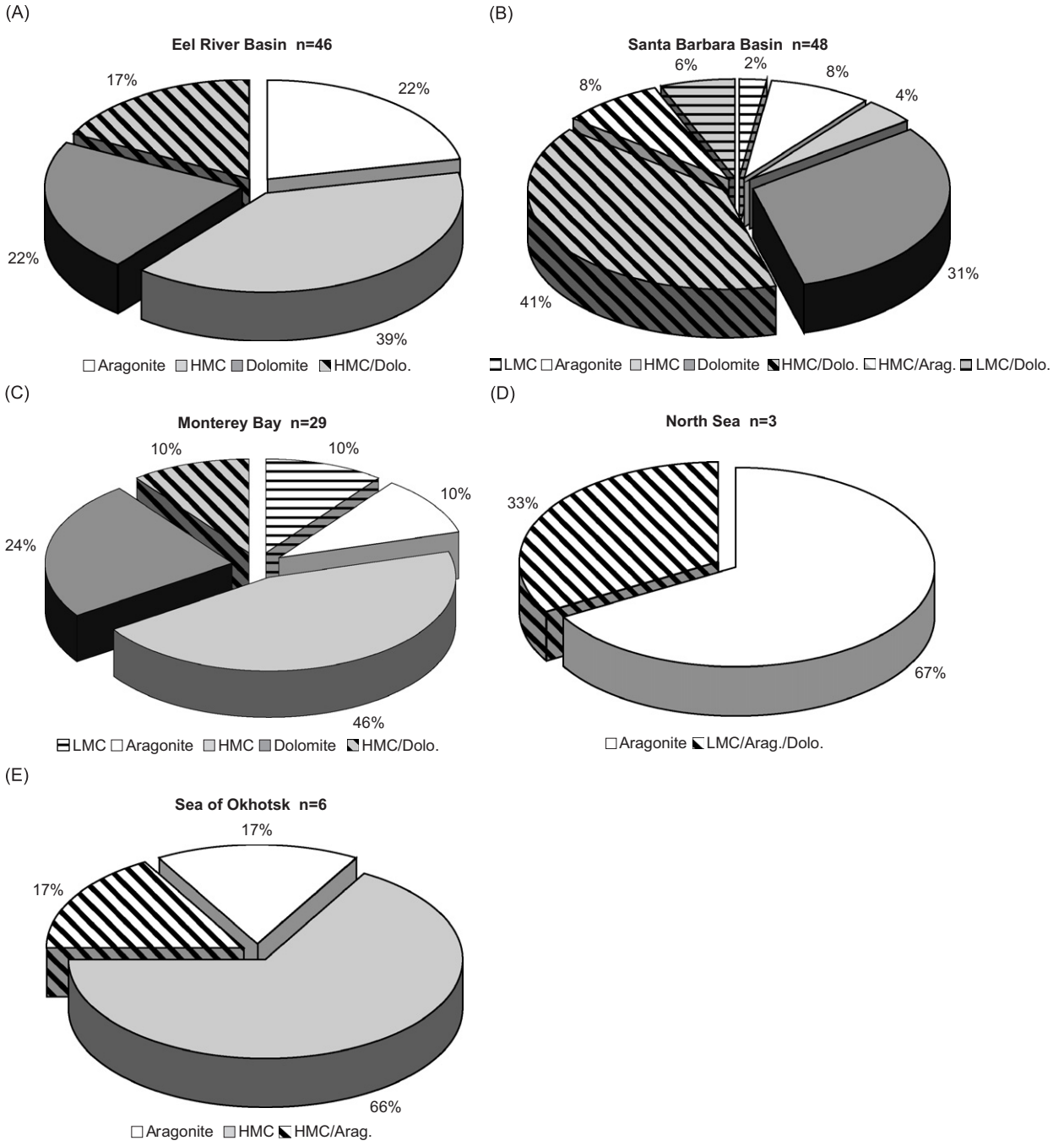

Fig. 2. Pie diagrams showing the distribution of different carbonate cements (aragonite, low-Mg calcite (LMC), high-Mg calcite (HMC), dolomite and mixtures thereof) within samples from the study areas. See text for further discussion.

$\varepsilon_{\text{gas hydrate/water}} \sim 3‰$; Davidson et al., 1983) in the subsurface. ^{18}O-depleted samples may indicate the influence of other factors, such as the local presence of meteoric water during carbonate precipitation.

Factors that influence which carbonate minerals precipitate at hydrocarbon seeps include the degree of carbonate supersaturation, the concentrations of Ca and Mg, the presence of complex forming anions

such as SO_4^{2-} and PO_4^{3-}, temperature, pCO_2, the degree of microbial activity, and the phylogeny of the microbes involved (Burton, 1993; Fernández-Díaz et al., 1996; Morse et al., 1997; Peckmann et al., 2001; Reitner et al., 2005). In general, high levels of carbonate supersaturation in combination with high Mg/Ca ratios seem to favor aragonite precipitation over the formation of Mg-calcite (Burton, 1993; Morse et al., 1997). Dolomite samples from hydrocarbon seep sites are commonly associated with high $\delta^{13}C$ values and are characteristic of the zone of methanogenesis, where CO_2 reduction and fractionation in a closed system pushes the carbon isotopic composition of the carbonates to $\delta^{13}C$ values of up to +25‰ or higher (Sample and Reid, 1998; Greinert et al., 2001; Orphan et al., 2004). The following discussion uses carbonate mineralogy and stable isotopic signatures of seep-related carbonates from the five study areas to distinguish between different biogeochemical processes that may lead to authigenic carbonate formation in hydrocarbon seep environments.

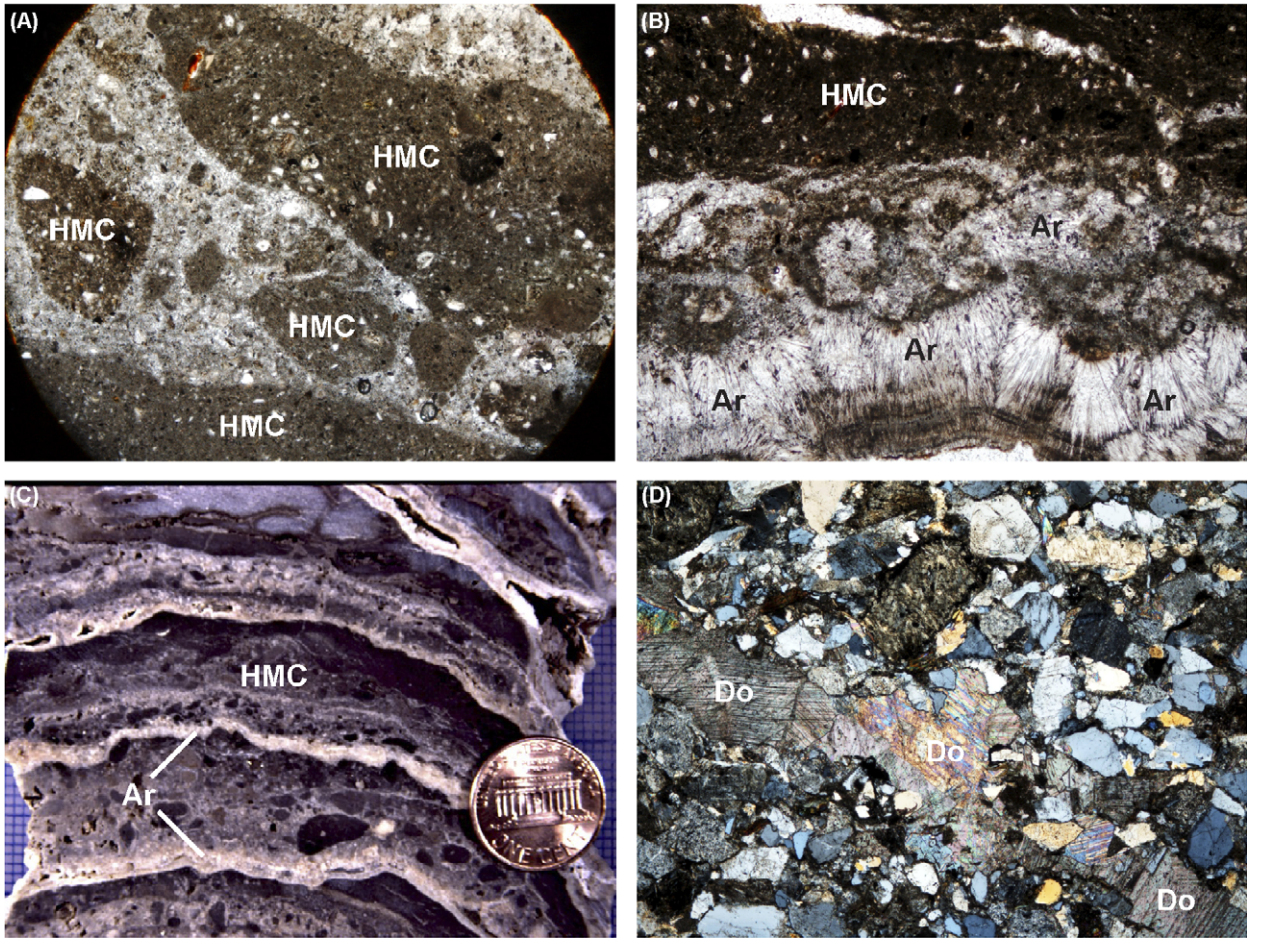

Fig. 3. Thin section photographs of representative samples from the study areas. (A) HMC-cemented intraclasts (dark) forming a brecciated texture in a sample from the Eel River Basin (sample 1307-RS-1a, plane polarized light, field of view 12 mm). (B) Co-occurrence of micritic HMC and sparitic aragonite within a single carbonate crust from the Eel River Basin (sample 1307-RS0-1b, plane polarized light, field of view 3 mm). (C) Textural relationship between HMC (dark gray) and aragonite (white) in hand specimen from the Eel River Basin. Aragonite represents a late-stage cement, filling voids between HMC-cemented regions of the sample (sample 1307-RS-1a, penny for scale). (D) Dolomite-cemented sandstone from the Eel River Basin (sample 1657-RS1, cross-polarized light, field of view 3 mm). (E) Sparitic aragonite cementing a void space in samples from Monterey Bay (sample 1088-RS-2a, cross-polarized light, field of view 1.2 mm). (F) Pyrite framboids filling the interior of a foraminifer test, indicating reducing conditions during carbonate precipitation (sample 738-RS-4, plane polarized light, field of view 0.6 mm). (G) Coarse-grained sample from the North Sea. Carbonate cements consist of micritic aragonite with minor amounts of LMC (sample TOM-98, cross-polarized light, field of view 3 mm). (H) Aragonite-cemented siltstone from the North Sea. Thin section was stained with Alizarin Red to show aragonite cement, previously identified by XRD (sample PM-204, plane polarized light, field of view 1.2 mm).

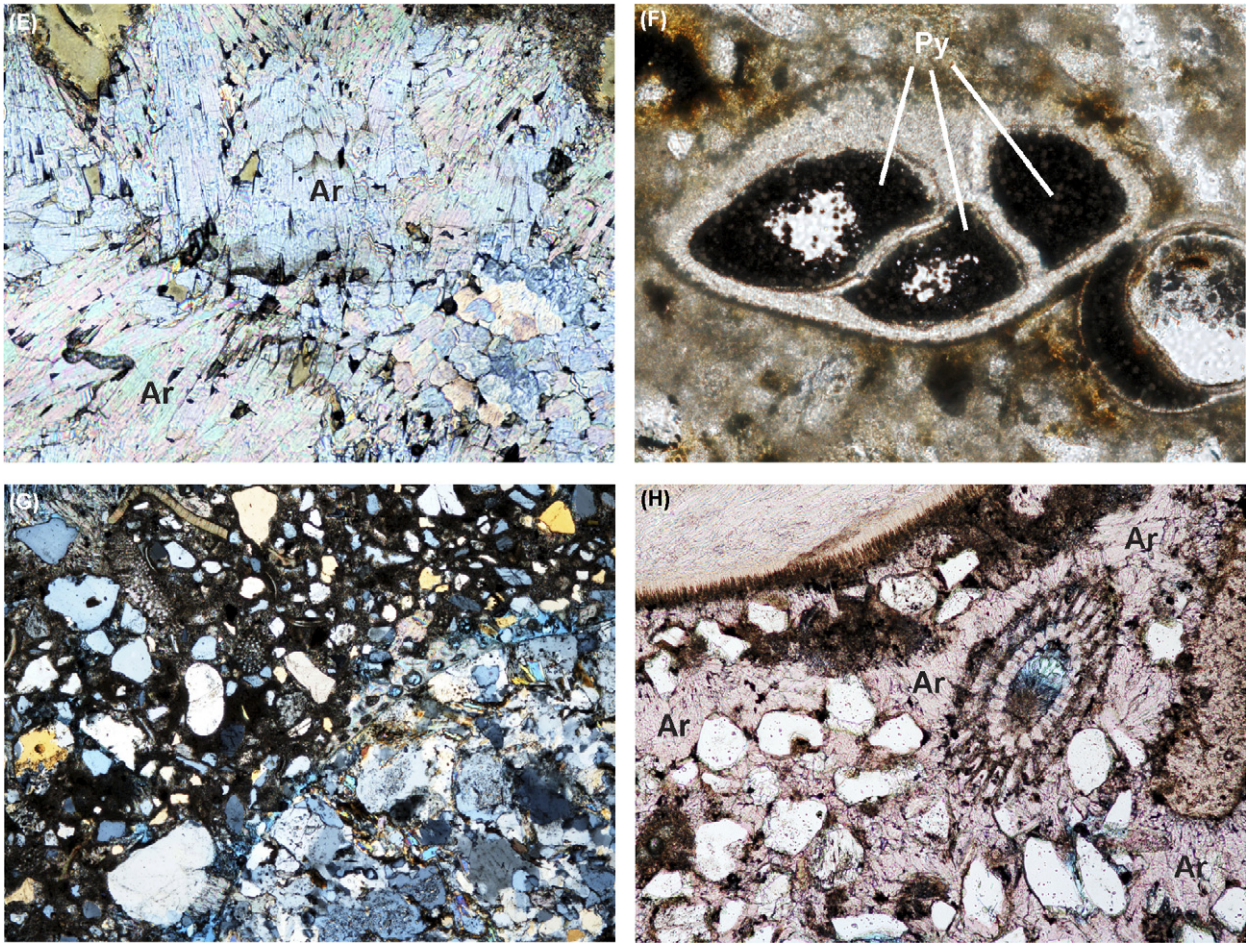

Fig. 3. (*Continued*)

5.1. Authigenic carbonate formation controlled by methane seepage

Areas of active methane seepage are characterized by AOM in the shallow subsurface, which leads to oversaturation of pore fluids with respect to carbonate and consequently precipitation of authigenic carbonate minerals (Eqs. (1) and (2)). The fact that methane oxidation is indeed one of the predominant geochemical processes at these sites can be demonstrated by using pore water $\delta^{13}C$ data for CO_2 and CH_4 from the Eel River Basin, which reveal CO_2–CH_4 carbon isotope fractionations between ~5‰ and 40‰, indicative for active methane oxidation in near-surface sediments (Fig. 5). Mixing of these strongly ^{13}C-depleted fluids and pore water with normal marine DIC or isotopically heavy CO_2 imprinted by methanogenesis in various proportions causes the observed large variations of carbonate $\delta^{13}C$ values in samples from all five study areas (Fig. 4). Accordingly, samples with $\delta^{13}C$ values below −5‰ and $\delta^{18}O$ values above 0‰ in Figs. 4 and 7 can be considered the result of authigenic carbonate precipitation in areas of active methane seepage.

Cements that form under such conditions are dominated by HMC and aragonite, although dolomite may also form in these environments (Stakes et al., 1999; Greinert et al., 2001). Authigenic nodules, slabs, and crusts are cemented by microcrystalline HMC, aragonite, or dolomite (Fig. 2). Samples from Monterey Bay and Eel River Basin commonly display two distinct cement generations characterized by early formation of micritic HMC, followed by a later, sparitic generation of aragonite. Framboidal pyrite is common in these rocks, confirming anoxic conditions during carbonate precipitation (Fig. 3F). The brecciated and

porous texture of many of these samples (Fig. 3B) suggests formation in the shallow subsurface. Elevated bicarbonate concentration in the pore fluids, fueled by AOM, will lead to the formation of HMC cements within the zone of sulfate reduction. Brecciation of these semi-consolidated,

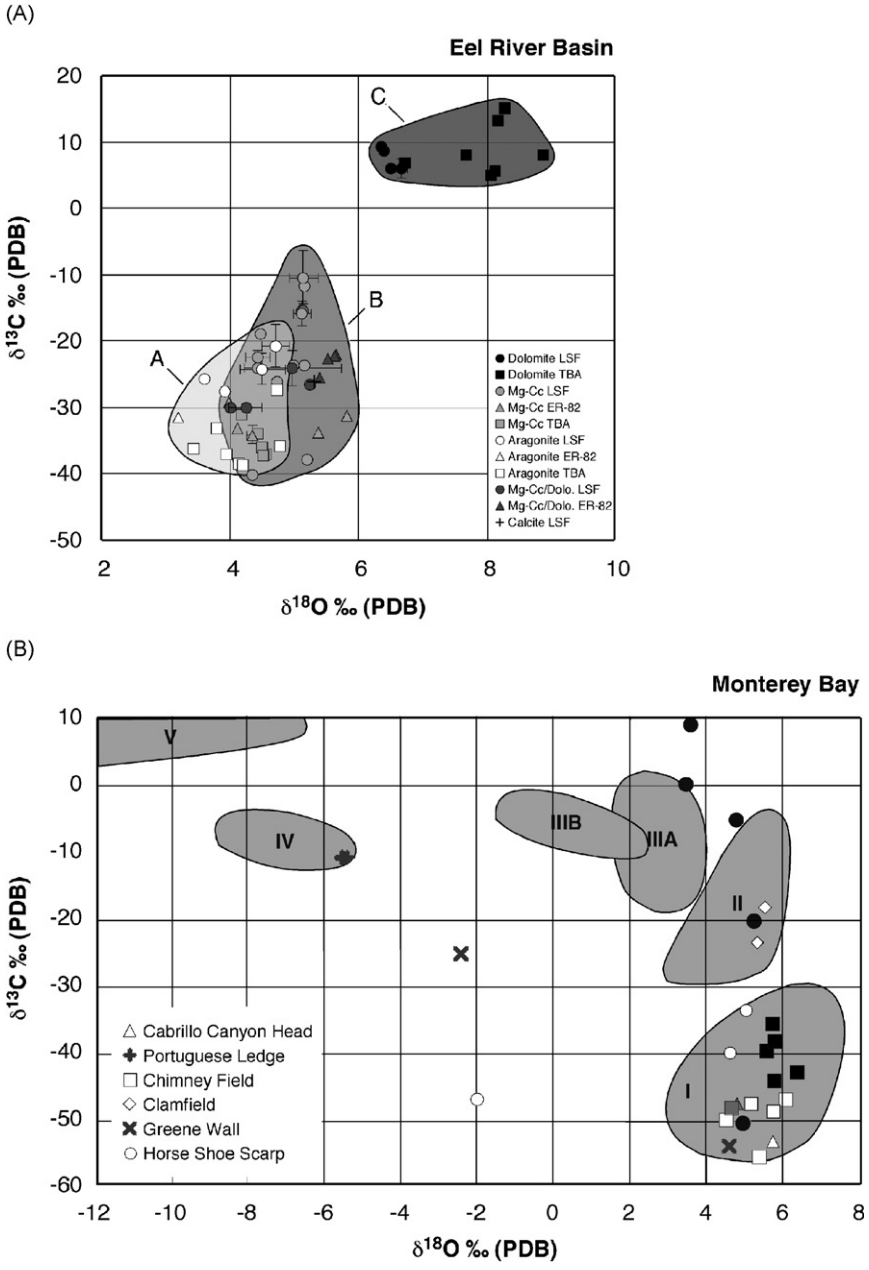

Fig. 4. Carbon and oxygen isotopic compositions for seafloor carbonates from Eel River Basin (ERB), Monterey Bay, the North Sea and Sea of Okhotsk, and Santa Barbara Basin (SBB). Open symbols: aragonite and low-Mg-calcite cements; gray filled symbols: HMC (light gray) or HMC/dolomite cements (dark gray); black filled symbols: dolomite cements. (A) ERB samples. Group A: aragonite-cemented seafloor carbonates; Group B: HMC-cemented and HMC/dolomite-cemented seafloor carbonates; Group C: dolomite-cemented seafloor carbonates with positive $\delta^{13}C$ values. LSF: Little Salmon fault; TBA: Table Bluff anticline. (B) Monterey Bay samples. Groups I–V for Monterey Bay seep carbonates from Stakes et al. (1999) are shown from comparison. (C) Santa Barbara Basin samples. Aragonite and HMC cements appear to be the result of methane oxidation, whereas $\delta^{13}C$ values of dolomite cements vary over a wide range, suggesting multiple carbon sources for seafloor carbonates from the Santa Barbara Basin. (D) North Sea and Sea of Okhotsk samples. All samples indicate carbonate precipitation resulting from AOM at sites of active hydrocarbon seepage. See text for further discussion.

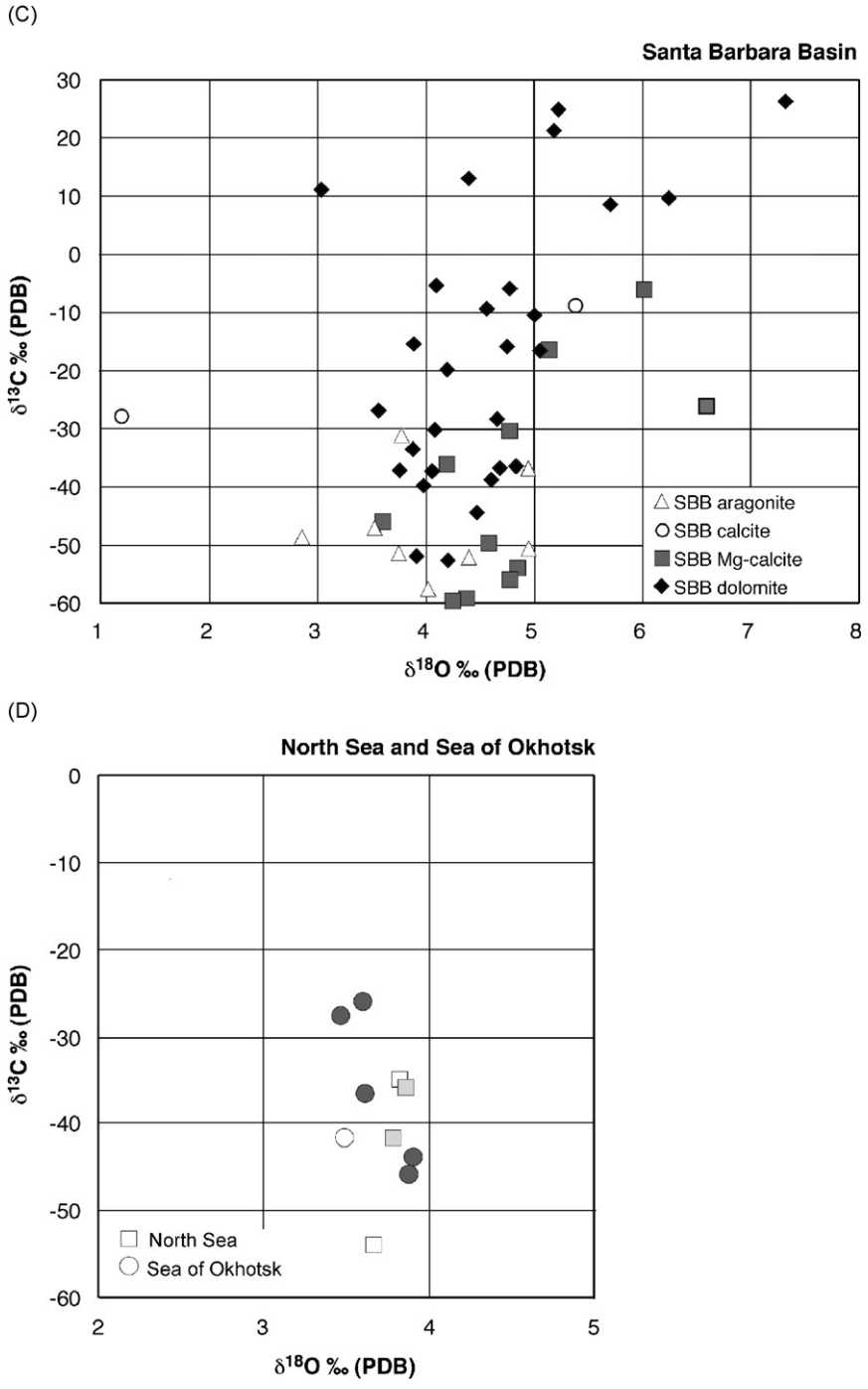

Fig. 4. (*Continued*)

HMC-cemented sediments may be triggered by tectonic or seepage-induced disturbances, such as rapidly increasing flow rates or the sudden release of trapped fluids and gases (Matsumoto, 1990; Greinert et al., 2001). Subsequent cementation by aragonite supports a second phase of carbonate precipitation in an environment characterized by higher sulfate concentrations, which would promote aragonite precipitation by inhibiting HMC crystallization (Burton, 1993; Savard et al., 1996). Such conditions may be present very close to or directly at the seafloor, where HCO_3^--rich fluids mix with

sulfate-rich bottom water. One process that could cause the observed bimodal distribution of carbonate cements is HMC precipitation at depths several meters below the sediment–water interface followed by regional uplift and erosion that would cause a steady upward migration of the samples in the sediment column and formation of aragonite close to the seafloor. The presence of authigenic slabs and crusts on the seafloor strongly supports a post-formational exhumation of these samples.

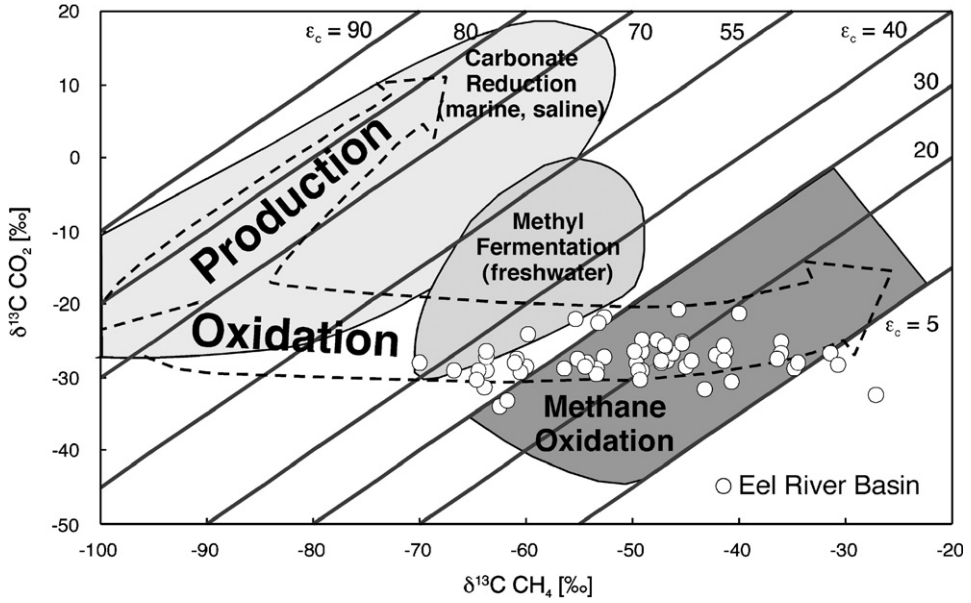

Fig. 5. Combination plot of $\delta^{13}C_{CH_4}$ and $\delta^{13}C_{CO_2}$ with isotope fractionation lines (ε_c) for pore water samples from the Eel River Basin (modified after Whiticar, 1999). Samples follow the expected CO_2–CH_4 carbon isotope partitioning trajectory resulting from microbial methane oxidation.

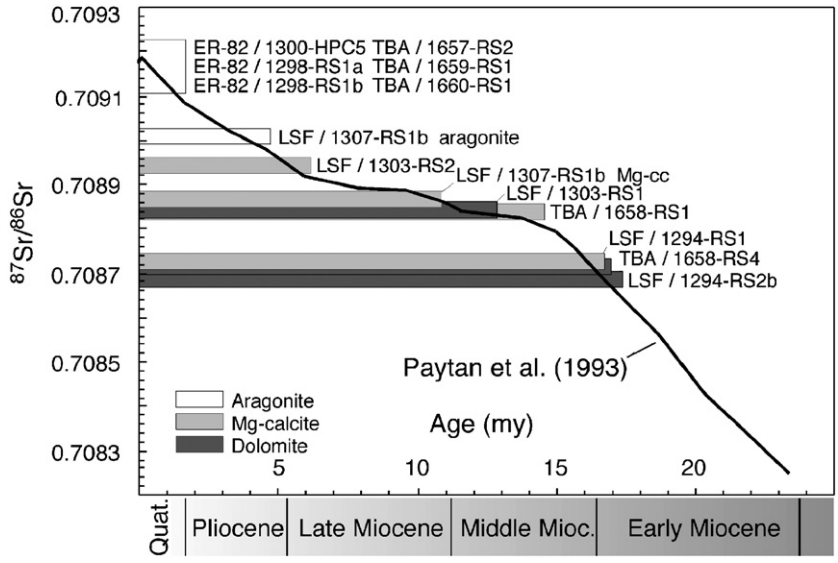

Fig. 6. Strontium isotope data for authigenic carbonates from the Eel River Basin. At least some of the carbonates appear to have formed from isotopically ''old'' pore fluids, which would indicate a deep-seated strontium source. Alternatively, the carbonates could have formed in the Geologic Past in contact with Miocene bottom water. Please note that the length of the bars in the diagram does not indicate the age of the respective carbonate samples but was merely chosen to intersect with the seawater Sr curve (after Paytan et al., 1993).

Sr-isotope data from Eel River Basin also point to aragonite formation in equilibrium with modern seawater, whereas less radiogenic values of HMC samples indicate Mg-calcite precipitation in contact with ^{87}Sr-depleted pore fluids derived from greater depth (Fig. 6). Alternatively, decreasing methane flux rates over time could produce a similar carbonate cement distribution by allowing the base of the sulfate reduction zone to migrate deeper into the sediment. Similar textural relationships and modes of authigenic carbonate formation have been reported from other areas of methane seepage as well (Naehr et al., 2000a; Greinert et al., 2001; Aloisi et al., 2002; Greinert et al., 2002; Gieskes et al., 2005). Carbonate-cemented mudstones dominated by HMC and dolomite from Monterey Bay (Stakes et al., 1999, Groups IIIA and IIIB) and Santa Barbara Basin are very likely examples of authigenic carbonate formation in the deepest part of the sulfate reduction zone, where low sulfate concentrations in the pore fluids and a lower degree of carbonate supersaturation facilitate the precipitation of Mg-rich carbonate minerals over aragonite (Burton, 1993; Greinert et al., 2001), which is typically absent in these samples.

As mentioned above, carbon isotopic compositions of seep-related carbonates vary widely, from about −5‰ to −57.5‰ (Fig. 4), indicating varying contributions from strongly ^{13}C-depleted, methane-derived carbon, carbon from degraded organic matter, and marine carbonate. It should be noted that the upper limit (−5‰) for this group is not a sharp boundary, but rather the end of a gradual transition from carbon isotopic values clearly produced by the anaerobic oxidation of biogenic methane (resulting in carbonate δ^{13}C values below −40‰) to isotopic signatures indicating the bacterial consumption of methane from thermogenic sources (∼−40‰ to −20‰) and increasing contributions of sedimentary organic and/or inorganic carbon (Naehr et al., 2000a; Orphan et al., 2004). Samples with very negative δ^{13}C values (below about −40‰), including many samples from Monterey Bay, Santa Barbara Basin, and the North Sea, are typically considered to have formed from the oxidation of microbially produced biogenic methane. Less ^{13}C-depleted carbonates, on the other hand, are indicative of oxidation of thermogenic methane and/or admixtures of dissolved inorganic carbon and CO_2 generated by decomposition of organic matter (Naehr et al., 2000a). It is likely that most of the less ^{13}C-depleted carbonate samples from the Sea of Okhotsk, Eel River Basin, and Monterey Bay have formed through the latter process (Martin et al., 1997). Monterey Bay samples from Clamfield and Horse Shoe Scarp with only moderately depleted δ^{13}C signatures plot in Group II of Stakes et al. (1999), and reflect the above-mentioned mixing of methane-derived and sedimentary organic and/or inorganic carbon (Fig. 7). Similarities can be drawn between carbonate samples from the Sea of Okhotsk near Sakhalin Island and those from the Eel River Basin. Both localities occur near onshore oil and gas production, and gas is actively venting from the seafloor. However, despite the proximity of thermogenic hydrocarbons to these localities, significant portions of the methane pool appear to be derived from microbial sources. The methane carbon isotopic composition of gas hydrate at both sites ranges from –58‰ to –69‰, suggesting a microbial source for methane (Lorenson et al., 1999). Seep gases from the Eel River Basin likely have mixed sources of hydrocarbons; they are nearly 100% methane (C_1) with $C_1/(C_2+C_3)$ ratios over 3500. However, trace amounts of thermogenic gases and methane carbon isotopic compositions ranging from −27‰ to −68‰ suggest mixed microbial and thermal sources (Orphan et al., 2004).

Oxygen isotopic data from authigenic carbonates are widely used to reconstruct mineral precipitation temperatures or, if bottom water temperatures are known, to infer the oxygen isotopic composition of the seeping fluids. However, such calculations must be applied with caution because even if the temperature and δ^{18}O composition of the surrounding fluids are known, one has to assume carbonate precipitation in thermodynamic equilibrium with the associated pore fluids. Furthermore, carbonate mineralogy, especially the incorporation of Mg into the crystal structure, will influence the isotopic fractionation of oxygen during mineral precipitation and needs to be taken into consideration when estimating crystallization temperatures and/or pore fluid compositions (Greinert et al., 2001). Assuming equilibrium crystallization of all carbonate minerals, methane-derived authigenic carbonates from Monterey Bay with δ^{18}O values between 4.52‰ and 6.37‰ for various carbonate mineralogies (aragonite, HMC, dolomite) would indicate temperatures of carbonate precipitation ranging from −4.6 °C (sample 1088-RS2A, HMC) to +7.5 °C (sample 1062-RS4, dolomite). Prevailing bottom water temperatures in Monterey Bay are in the range of

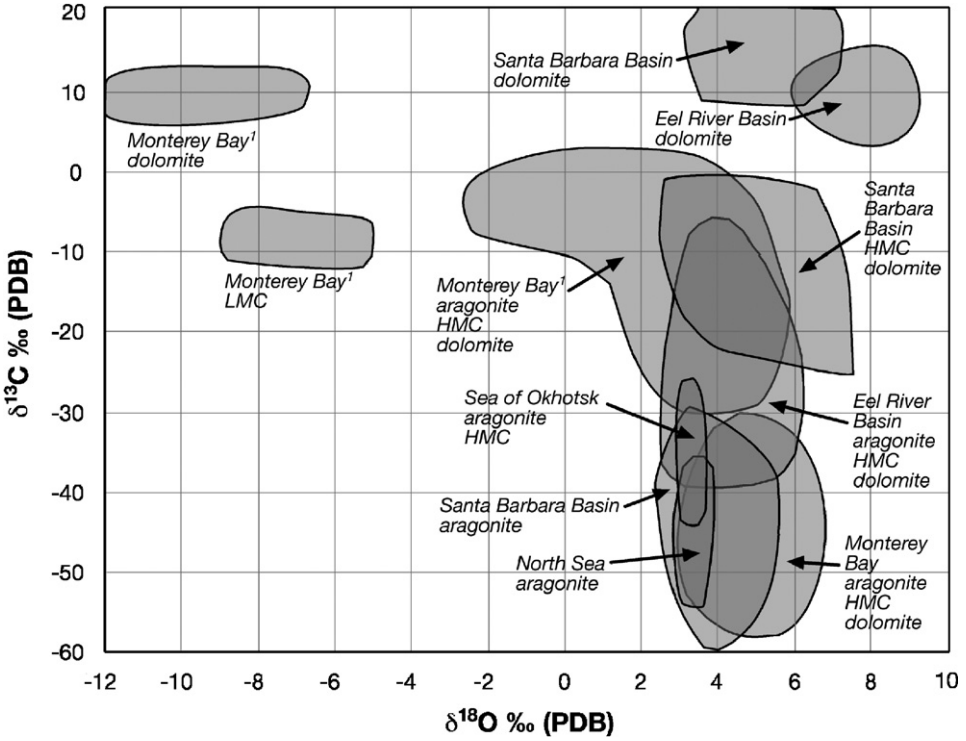

Fig. 7. Carbon and oxygen isotopic composition summary plot for seafloor carbonates from all study areas. The carbon isotopic data indicate complex carbon sources from both ^{13}C-depleted (Mg calcite, aragonite) and residual, ^{13}C-enriched (dolomite), carbon pools. Although found on the seafloor, isotopically heavy dolomites do not seem to be related to shallow methane oxidation at the seep sites. The δ^{18}O data for authigenic high-Mg calcite and aragonite show values as high as +6.6‰ and +4.9‰, respectively (SBB samples 1507-4 and 156-4), pointing toward a heavy, ^{18}O-enriched oxygen source for some of the samples, possibly related to the advection of ^{18}O-enriched formation water or to the decomposition of gas hydrate.

3–4 °C, suggesting carbonate precipitation in isotopic disequilibrium at least for samples at the extreme ends of the calculated temperature spectrum. Alternatively, pore fluid δ^{18}O compositions varying over a range from about −1‰ to +2.5‰ (vs. SMOW) would be required to calculate carbonate formation temperatures of 3–4 °C. No such data have been reported for Monterey Bay and natural pore water δ^{18}O variations of ±3.5‰ are not likely to occur in such a relatively restricted area, especially in the absence of gas hydrate deposits.

In the Eel River Basin, δ^{18}O values for HMC and HMC/dolomite cements vary between 3.98‰ and 5.84‰, indicating carbonate precipitation temperatures of +3.4 to −3.8 °C assuming a pore fluid composition of 0‰ SMOW. Temperatures below 0 °C are clearly unrealistic, especially when compared to measured bottom water temperatures of 5.5 °C at the time of our ROV dives. Therefore, a contribution of isotopically heavier pore fluids has to be assumed. Using 5.5 °C as the ambient temperature during carbonate formation, a pore fluid oxygen isotopic composition of +0.6‰ to +2.5‰ SMOW would be required for equilibrium precipitation of HMC (Fig. 8A). Such positive values would indicate a contribution of ^{18}O-enriched water, presumably due to gas hydrate decomposition (Hesse and Harrison, 1981; Greinert et al., 2001). Pore water samples collected during our 1997 dives did show δ^{18}O values of +0.6‰ SMOW, which may account for at least part of the required ^{18}O enrichment of the pore fluids. Aragonite samples from Eel River ($\delta^{18}O_{aragonite}$ 3.2–4.8‰) point to mineral precipitation in equilibrium with pore fluids closer to SMOW (+0.5‰ to +1.5‰ at 5.5 °C; Fig. 8B), but still enriched in ^{18}O. Brooks et al. (1991) reported the occurrence of gas hydrate in piston cores from the Eel River Basin. Decomposition of these near-surface deposits would release methane and ^{18}O-enriched water that could explain the observed carbonate δ^{18}O values.

Authigenic aragonite from Santa Barbara Basin shows a similar range of δ^{18}O values (2.8–4.9‰), resulting in pore fluid estimates of −0.1‰ to +2.0‰ SMOW at modern bottom water temperatures of

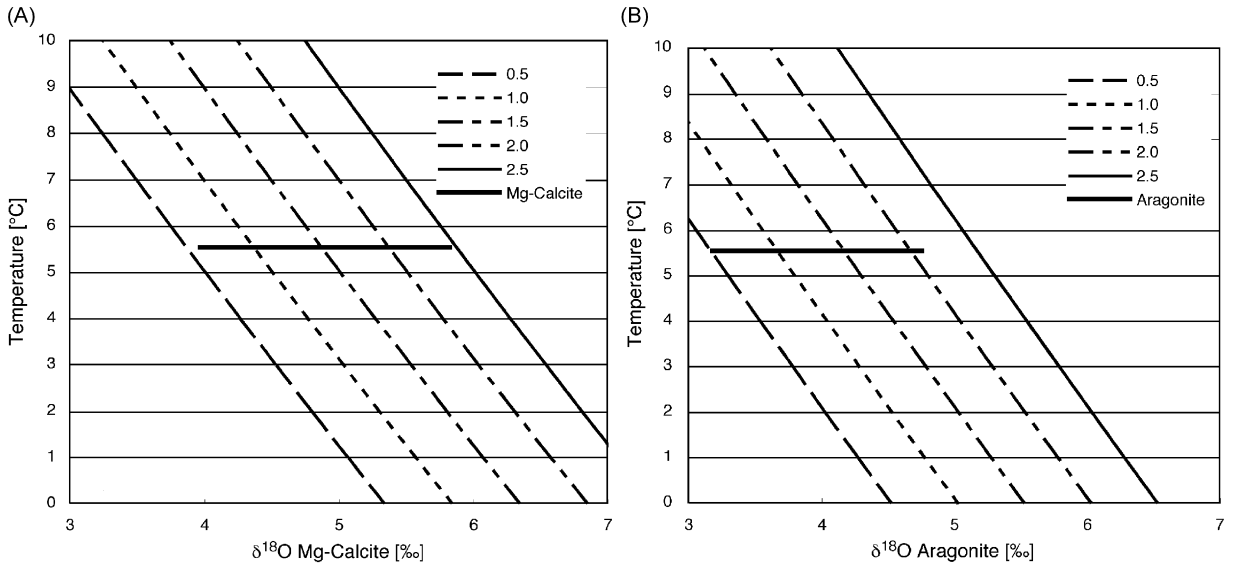

Fig. 8. Temperature–$\delta^{18}O$ plots illustrating the range of pore water compositions required for equilibrium crystallization of carbonate samples from the Eel River Basin. (A) Plot for high-Mg calcite at a bottom water temperature of 5.5 °C. Diagonal lines: hypothetical oxygen isotopic composition of pore fluids required for equilibrium crystallization of HMC with $\delta^{18}O$ values ranging from +4.0‰ to +5.8‰ (after Hudson and Anderson, 1989). (B) Plot for aragonite at a bottom water temperature of 5.5 °C. Diagonal lines: hypothetical oxygen isotopic composition of pore fluids required for equilibrium crystallization of aragonite with $\delta^{18}O$ values ranging from +3.2‰ to +4.8‰ (after Friedman and O'Neil, 1977).

approximately 7 °C. A contribution of ^{18}O-enriched formation water derived from greater depth may explain these elevated oxygen isotope values (Eichhubl and Boles, 1998; Eichhubl et al., 2000). Finally, oxygen isotopic values of samples from the North Sea and Sea of Okhotsk vary over a much smaller range (North Sea: 3.7–3.8‰; Sea of Okhotsk: 3.5–3.9‰), signaling carbonate precipitation at temperatures of 3.1–3.8 °C and 1.0–1.4 °C, respectively. Assuming bottom water compositions of 0‰ SMOW for the North Sea and using published values of −0.5‰ for the Sea of Okhotsk (Greinert et al., 2002), carbonates from the Sea of Okhotsk appear to have formed in equilibrium with prevailing bottom water temperatures, whereas precipitation temperatures for the North Sea samples appear a bit low given a bottom water temperature range of 4–6 °C in the study area. However, Sr-isotope ratios for these samples, which are comparable to modern seawater, corroborate recent carbonate precipitation close to the sediment–water interface.

5.2. *Authigenic carbonate formation not related to methane seepage*

Authigenic carbonates unrelated to methane seepage are represented by LMC and dolomite samples from Monterey Bay (Stakes et al., 1999, Groups IV and V) and dolomites from Santa Barbara and Eel River Basin with positive $\delta^{13}C$ or clearly negative $\delta^{18}O$ values (Fig. 7). Positive $\delta^{13}C$ values in dolomitic cements from Eel River Basin (+5.0‰ to +15.1‰) and Santa Barbara Basin (+8.6‰ to +26.3‰) are most likely related to methanogenesis and were caused by carbonate formation from a carbon reservoir where the preferential removal of ^{12}C from the DIC pool to form CH_4 leaves the residual carbon reservoir ^{13}C enriched (Stakes et al., 2002; Gieskes et al., 2005). The oxygen isotopic composition of ^{12}C-depleted dolomites from the Eel River Basin suggests temperatures of carbonate precipitation between 4 and 9 °C. These slightly elevated temperatures support a model of dolomite formation at greater depth, followed by subsequent uplift, erosion, and exposure on the seafloor (Orphan et al., 2004). The $\delta^{18}O$ values of corresponding dolomite samples from Santa Barbara basin (+3.0‰ to +7.3‰ at pore fluid $\delta^{18}O$ values of > +2‰; Eichhubl and Boles, 1998) indicate even higher temperatures for dolomite formation of 7.2–26.4 °C, again supporting a model of carbonate precipitation at depth, followed by exhumation, possibly accompanied by uplift. Samples 1490-1–1490-7 are texturally,

lithologically, and isotopically similar to dolostone of the Miocene Monterey Formation that is exposed along the Santa Barbara coast. Analyses by Eichhubl and Boles (1998) provided $\delta^{18}O$ values of 1.2–2.9‰ PDB and $\delta^{13}C$ values of 8.7–13.5‰ PDB, consistent with similar Monterey dolostone analyses by Winter and Knauth (1992). In their detailed analysis of Monterey dolostone, Burns and Baker (1987) interpreted these isotopically heavy dolostones to reflect fractionation during methanogenesis, producing isotopically light methane and heavy residual pore water bicarbonate. We thus infer that samples 1490-1–1490-7 are reworked Monterey dolostone samples, which is consistent with the rounded shape of these samples. Based on a detailed burial reconstruction, Eichhubl and Boles (1998) inferred an exhumation of 750 m for the nearby coastal dolostone exposures.

Authigenic carbonates from Monterey Bay with clearly negative $\delta^{18}O$ values ranging from −5.4‰ to −5.8‰ and $\delta^{13}C$ values of around −11‰ most likely formed under influence of meteoric water, either as primary precipitates or through recrystallization of seep carbonates under meteoric conditions. Stakes et al. (1999) used a $\delta^{18}O$ composition of −8‰ SMOW to calculate temperatures of carbonate formation of 12–16 °C for samples from the same location (Portuguese Ledge) and proposed that the site might have been subaerially exposed during the last sealevel lowstand (current water depth: 86 m). In any case, the stable isotopic composition of these samples clearly argues against any relationship to hydrocarbon seepage.

It should be pointed out that in three of the five areas presented in this study, carbonate concretions and slabs unrelated to processes driven by the AOM occur on the seafloor, often in close proximity to and visually undistinguishable from AOM-derived carbonates. There are two main conclusions that can be drawn from this observation: (1) all three areas must have undergone erosion and uplift in the past or are still being uplifted. Since these areas (Monterey Bay, Eel River Basin, and Santa Barbara Basin) are all located on an active continental margin with transform or transpressional tectonics (Mount and Suppe, 1992; Orange, 1999; Eichhubl et al., 2000), this is not an unlikely scenario. (2) The occurrence of carbonate slabs on the seafloor in areas of active hydrocarbon seepage does not necessarily mean that all seafloor carbonates are the result of AOM that dominates these environments. Care must be taken during collection and analysis of carbonate rocks from areas of active or past hydrocarbon seepage.

6. Conclusions

Authigenic carbonates from five study areas exhibit a wide range of mineralogical and stable isotopic compositions. The mineralogy of these precipitates ranges from HMC and aragonite to dolomite. The carbon isotopic composition of carbonates varies widely, indicating complex carbon sources from both ^{13}C-depleted and residual, ^{13}C-enriched, bicarbonate. The large variability of $\delta^{18}O$ values also demonstrates the geochemical complexity of these sites with some samples pointing toward a heavy, $\delta^{18}O$-enriched oxygen source possibly related to the advection of ^{18}O-enriched formation water or to the decomposition of gas hydrate, whereas ^{18}O-depleted samples may indicate carbonate precipitation deeper in the sediment or the local presence of meteoric water during carbonate precipitation.

A wide range of isotopic and mineralogical variation in authigenic carbonate composition within individual study areas but common trends across multiple geographic areas suggest that these parameters alone are not indicative for certain tectonic or geochemical settings. Rather, the observed variations probably reflect local controls on the flux of carbon and other reduced ions, such as faults, fluid conduits, the presence or absence of gas hydrate in the sediment, and the temporal evolution of the local carbon reservoir.

Areas with seafloor carbonates that indicate formation at greater depth below the sediment–water interface, like many of the dolomite samples with positive $\delta^{13}C$ and/or negative $\delta^{18}O$ values, must have undergone uplift and erosion in the past or are still being uplifted. Consequently, the occurrence of carbonate slabs on the seafloor in areas of active hydrocarbon seepage is commonly an indicator of exhumation following carbonate precipitation in the shallow subsurface. Therefore, careful petrographic and geochemical analyses are critical components necessary for the correct interpretation of processes related to hydrocarbon seepage in continental margin environments and elsewhere.

Acknowledgments

We thank the captain and crew of R/V *Point Lobos* and the pilots of ROV *Ventana* for their dedicated efforts to obtain many of the samples

used in this study. We also thank G. Bohrmann, J. Greinert, D. Orange, D. Stakes, J. Martin, and many other colleagues for years of stimulating discussions. We are grateful for the comments provided by J. Peckmann and an anonymous reviewer, which greatly improved the paper. We also thank M. Dalthorp for her critical remarks and C. Glenn and G. Filippelli for the editorial handling of the paper. Financial support for this study was provided by the David and Lucile Packard Foundation, the Monterey Bay Aquarium Research Institute, through a TAMUCC Faculty Summer Research Grant, and NSF-EAR award 0421410.

References

Aiello, I.W., 2005. Fossil seep structures of the Monterey Bay region and tectonic/structural controls on fluid flow in an active transform margin. Palaeogeography, Palaeoclimatology, Palaeoecology 227 (1–3), 124–142.

Alexander, C.R., Simoneau, A.M., Nittrouer, C.A., 1999. Spatial variability in sedimentary processes on the Eel continental slope. Marine Geology 154, 243–254.

Allen, A.A., Schlueter, R.S., Mikolaj, P.G., 1970. Natural oil seepage at Coal Oil Point, Santa Barbara, California. Science 170 (3961), 974–977.

Aloisi, G., Bouloubassi, I., Heijs, S.K., Pancost, R.D., Pierre, C., Sinninghe Damste, J.S., Gottschal, J.C., Forney, L.J., Rouchy, J.-M., 2002. CH_4-consuming microorganisms and the formation of carbonate crusts at cold seeps. Earth and Planetary Science Letters 203 (1), 195–203.

Astakhova, N.V., 1997. Barite mineralization in sediments of the West Pacific marginal seas. Geology of the Pacific Ocean 13, 945–955.

Baker, P.A., Burns, S.J., 1985. Occurrence and formation of dolomite in organic-rich continental margin sediments. AAPG Bulletin 69 (11), 1917–1930.

Barry, J.P., Greene, H.G., Orange, D.L., Baxter, C.H., Robinson, B.H., Kochevar, R.E., Nybakken, J.W., Reed, D.L., McHugh, C.M., 1996. Biologic and geologic characteristics of cold seeps in Monterey Bay, California. Deep-Sea Research I 43 (11–12), 1739–1762.

Brooks, J.M., Field, M.E., Kennicutt II, M.C., 1991. Observations of gas hydrates in marine sediments, offshore northern California. Marine Geology 96, 103–109.

Burns, S.J., Baker, P.A., 1987. A geochemical study of dolomite in the Monterey Formation, California. Journal of Sedimentary Petrology 57, 128–139.

Burton, E.A., 1993. Controls on marine carbonate cement mineralogy: review and reassessment. Chemical Geology 105, 163–179.

Burton, E.A., Walter, L.M., 1991. The effects of P_{CO_2} and temperature on magnesium incorporation in calcite in seawater and $MgCl_2$–$CaCl_2$ solutions. Geochimica et Cosmochimica Acta 55, 777–785.

Carver, G.A., 1987. Late Cenozoic tectonics of the Eel River Basin region, coastal Northern California. In: Schymiczek, H., Suchsland, R. (Eds.), Tectonics, Sedimentation and Evolution of the Eel River and Associated Coastal Basins of Northern California. San Joaquin Geological Society, Bakersfield, CA, pp. 61–71.

Clarke Jr., S.H., 1992. Geology of the Eel River Basin and adjacent region; implications for Late Cenozoic tectonics of the southern Cascadia subduction zone and Mendocino triple junction. AAPG Bulletin 76 (2), 199–224.

Claypool, G.E., Kaplan, I.R., 1974. The origin and distribution of methane in marine sediments. In: Kaplan, I.R. (Ed.), Natural Gases in Marine Sediments. Plenum Press, New York, London, pp. 99–139.

Davidson, D.W., Leaist, G., Hesse, R., 1983. Oxygen-18 enrichment in the water of a clathrate hydrate. Geochimica et Cosmochimica Acta 47, 2293–2295.

D'Heur, M., Pekot, L.J., Spencer, A.M., 1987. Tommeliten. In: Spencer, A.M. (Ed.), Geology of the Norwegian Oil and Gas Fields. Graham & Trotman, Norwell, MA, London, pp. 117–128.

Eichhubl, P., Behl, R.J., 1998. Diagenesis, deformation, and fluid flow in the Miocene Monterey Formation: Ventura–Santa Barbara–Jalama Beach–Grefco Quarry/Lompoc. In: Eichhubl, P. (Ed.), SEPM Pacific Section Special Publication. Society of Economic Paleontologists and Mineralogists, Pacific Section, Los Angeles, CA, pp. 85–98.

Eichhubl, P., Boles, J.R., 1998. Vein formation in relation to burial diagenesis in the Miocene Monterey Formation, Arroyo Burro Beach, Santa Barbara, California. In: Eichhubl, P. (Ed.), Diagenesis, Deformation, and Fluid Flow in the Miocene Monterey Formation of Coastal California, pp. 15–36.

Eichhubl, P., Boles, J.R., 2000. Focused fluid flow along faults in the Monterey Formation, coastal California. Geological Society of America Bulletin 112 (11), 1667–1679.

Eichhubl, P., Greene, H.G., Naehr, T., Maher, N., 2000. Structural control of fluid flow; offshore fluid seepage in the Santa Barbara Basin, California. Journal of Geochemical Exploration 69–70, 545–549.

Elvert, M., Suess, E., 1999. Anaerobic methane oxidation associated with marine gas hydrates: superlight C-isotopes from saturated and unsaturated C20 and C25 irregular isoprenoids. Naturwissenschaften 86, 295–300.

Fernández-Díaz, L., Putnis, A., Prieto, M., Putnis, C.v., 1996. The role of magnesium in the crystallization of calcite and aragonite in a porous medium. Journal of Sedimentary Research 66 (3), 482–491.

Friedman, I., O'Neil, J.R., 1977. Compilation of stable isotope fractionation factors of geochemical interest. In: Fleischer, M. (Ed.), Data of Geochemistry, sixth ed. U.S.G.S Professional Paper, 440-KK.

Gieskes, J., Mahn, C., Day, S., Martin, J.B., Greinert, J., Rathburn, T., McAdoo, B., 2005. A study of the chemistry of pore fluids and authigenic carbonates in methane seep environments: Kodiak Trench, Hydrate Ridge, Monterey Bay, and Eel River Basin. Chemical Geology 220 (3–4), 329–345.

Ginsburg, G.D., Soloviev, V.A., Cranston, R.E., Lorenson, T.D., Kvenvolden, K.A., 1993. Gas hydrates from the continental slope, offshore Sakhalin Island, Okhotsk Sea. Geo-Marine Letters 13, 41–48.

Goldsmith, J.R., Graf, D.L., Heard, H.C., 1961. Lattice constants of the calcium–magnesium carbonates. American Mineralogist 46, 453–457.

Greene, H.G., 1977. Geology of the Monterey Bay region. U.S. Geological Survey Open-File Report 77-718, p. 347.

Greene, H.G., 1990. Regional tectonics and structural evolution of the Monterey Bay region, Central California. In: Greene, H.G., Weber, G.E., Wright, T.L. (Eds.), Geology and Tectonics of the Central California Coast Region, San Francisco to Monterey: Volume and Guidebook. Pacific Section of the American Association of Petroleum Geologists, Bakersfield, CA, pp. 205–228.

Greinert, J., Derkachev, A., 2004. Glendonites and methane-derived Mg-calcites in the Sea of Okhotsk, Eastern Siberia: implications of a venting-related ikaite/glendonite formation. Marine Geology 204 (1–2), 129–144.

Greinert, J., Bohrmann, G., Suess, E., 2001. Gas hydrate-associated carbonates and methane-venting at Hydrate Ridge: classification, distribution and origin of authigenic lithologies. In: Paull, C.K., Dillon, W.P. (Eds.), Natural Gas Hydrates: Occurrence, Distribution, and Detection. American Geophysical Union, Washington, DC, pp. 99–113.

Greinert, J., Bollwerk, S.M., Derkachev, A., Bohrmann, G., Suess, E., 2002. Massive barite deposits and carbonate mineralization in the Derugin Basin, Sea of Okhotsk: precipitation processes at cold seep sites. Earth and Planetary Science Letters 203 (1), 165–180.

Hein, J.R., Normark, W.R., McIntyre, B.R., Lorenson, T.D., Powell, C.L.III., 2006. Methanogenic calcite, ^{13}C-depleted bivalve shells, and gas hydrate from a mud volcano offshore Southern California. Geology 34 (2), 109–112.

Hesse, R., Harrison, W.E., 1981. Gas hydrates (clathrates) causing pore-water freshening and oxygen isotope fractionation in deep-water sedimentary sections of terrigenous continental margins. Earth and Planetary Science Letters 55 (3), 453–462.

Hinrichs, K.-U., Hayes, J.M., Sylva, S.P., Brewer, P.G., DeLong, E.F., 1999. Methane-consuming archeabacteria in marine sediments. Nature 398, 802–805.

Horan III, E.P., Hopps, T.E., 1987. Exploration potential; onshore Eel River Basin, Humboldt County, California. In: Schymiczek, H., Suchsland, R. (Eds.), Tectonics, Sedimentation and Evolution of the Eel River and Associated Coastal Basins of Northern California. San Joaquin Geological Society, Bakersfield, CA, pp. 73–82.

Hoskins, E.G., Griffiths, J.R., 1971. Hydrocarbon potential of northern and central california offshore. In: Cram, I.H. (Ed.), Future Petroleum Provinces of the United States; Their Geology and Potential, vol. 1, pp. 212–228.

Hovland, M., 2002. On the self-sealing nature of marine seeps. Continental Shelf Research 22, 2387–2394.

Hovland, M., Sommerville, J.H., 1985. Characteristics of two natural gas seepages in the North Sea. Marine and Petroleum Geology 2 (4), 319–326.

Hovland, M., Talbot, M., Olaussen, S., Aasberg, L., 1985. Recently formed methane-derived carbonates from the North Sea floor. In: Thomas, B.M., Dore, A.G., Eggen, S.S., Home, P.C., Larsen, R.M. (Eds.), Petroleum Geochemistry in Exploration of the Norwegian Shelf. Graham & Trotman, London, UK, pp. 263–266.

Hovland, M., Judd, A.G., Burke Jr., R.A., 1993. The global flux of methane from shallow submarine sediments. Chemosphere 26 (1–4), 559–578.

Hudson, J.C., Anderson, T.F., 1989. Ocean temperatures and isotopic compositions through time. In: Clarkson, E.N.K., Curry, G.B., Rolfe, W.D.I. (Eds.), Environments and Physiology of Fossil Organisms. Edinburgh, pp. 183–192.

Irwin, H., 1980. Early diagenetic carbonate precipitation and pore fluid migration in the Kimmeridge Clay of Dorset, England. Sedimentology 27 (5), 577–591.

Kastner, M., Elderfield, H., Martin, J.B., Suess, E., Kvenvolden, K.A., Garrison, R.E., 1990. Diagenesis and interstitial-water chemistry at the peruvian continental margin—major constituents and strontium isotopes. In: Suess, E., von Huene, R. (Eds.), Proceedings of the Ocean Drilling Program, Scientific Results. Ocean Drilling Program, College Station, TX, pp. 413–440.

Leithold, E.L., Hope, R.S., Nittrouer, C.A., 1999. Deposition and modification of a flood layer on the Northern California shelf; lessons from and about the fate of terrestrial particulate organic carbon. Marine Geology 154, 183–195.

Lorenson, T.D., Naehr, T.H., Orange, D.L., 1999. Gas seeps and associated gas hydrate of the Okhotsk Sea near Sakhalin Island, Russia, and Eel River basin, Northern California; a comparison of gas and carbonate geochemistry. In: 1999 AAPG Pacific Section Meeting; Abstracts. AAPG Bulletin 695.

Luff, R., Wallmann, K., Aloisi, G., 2004. Numerical modeling of carbonate crust formation at cold vent sites: significance for fluid and methane budgets and chemosynthetic biological communities. Earth and Planetary Science Letters 221 (1–4), 337.

Lumsden, D.N., 1979. Error in X-ray diffraction estimates of dolomite in carbonate rocks—causes and cures. AAPG Bulletin 63 (3), 488.

Martin, J.B., Orange, D.L., Lorenson, T.D., Kvenvolden, K.A., 1997. Chemical and isotopic evidence of gas-influenced flow at a transform plate boundary; Monterey Bay, California. Journal of Geophysical Research 102 (B11), 24903–24915.

Martin, J.B., Day, S.A., Rathburn, A.E., Perez, M.E., Mahn, C., Gieskes, J., 2004. Relationships between the stable isotopic signatures of living and fossil foraminifera in Monterey Bay, California. Geochemistry, Geophysics, Geosystems 5 (4), 1.

Matsumoto, R., 1989. Isotopically heavy oxygen-containing siderite derived from the decomposition of methane hydrate. Geology 17 (8), 707–710.

Matsumoto, R., 1990. Vuggy carbonate crust formed by hydrocarbon seepage on the continental shelf of Baffin Island, northeast Canada. Geochemical Journal 24, 143–158.

McCulloch, D.S., Clarke Jr., S.H., Field, M.E., Scott, E.W., Utter, P.M., 1977. A summary report of the regional geology, petroleum potential, and environmental geology of the southern proposed lease sale 53, central and northern California outer continental shelf. Open-File Report, U.S. Geological Survey, p. 57.

Morse, J.W., Wang, Q., Tsio, M.Y., 1997. Influence of temperature and Mg:Ca ratio on $CaCO_3$ precipitates from seawater. Geology 25 (1), 85–87.

Mount, V.S., Suppe, J., 1992. Present-day stress orientations adjacent to active strike-slip faults: California and Sumatra. Journal of Geophysical Research 97 (B8), 11995–12013.

Naehr, T.H., Rodriguez, N.M., Bohrmann, G., Paull, C.K., Botz, R., 2000a. Methane-derived authigenic carbonates associated with gas hydrate decomposition and fluid venting above the Blake Ridge Diapir. In: Paull, C.K., Matsumoto, R., Wallace, P.J., Dillon, W.P. (Eds.), Proceedings of the Ocean Drilling

Program, Scientific Results. Ocean Drilling Program, College Station, TX, pp. 285–300.

Naehr, T.H., Stakes, D.S., Moore, W.S., 2000b. Mass wasting, ephemeral fluid flow, and barite deposition on the California continental margin. Geology 28 (4), 315–318.

Niemann, H., Elvert, M., Hovland, M., Orcutt, B., Judd, A., Suck, I., Gutt, J., Joye, S., Damm, E., Finster, K., Boetius, A., 2005. Methane emission and consumption at a North Sea gas seep (Tommeliten area). Biogeosciences 2, 335–351.

Orange, D.L., 1999. Tectonics, sedimentation, and erosion in northern California: submarine geomorphology and sediment preservation potential as a result of three competing processes. Marine Geology 154, 369–382.

Orange, D.L., Greene, H.G., Reed, D., Martin, J.B., McHugh, C.M., Ryan, W.B.F., Maher, N., Stakes, D., Barry, J., 1999. Widespread fluid expulsion on a translational continental margin: mud volcanoes, fault zones, headless canyons, and organic-rich substrate in Monterey Bay, California. Geological Society of America Bulletin 111 (7), 992–1009.

Orphan, V.J., Ussler III, W., Naehr, T.H., House, C.H., Hinrichs, K.-U., Paull, C.K., 2004. Geological, geochemical, and microbiological heterogeneity of the seafloor around methane vents in the Eel River Basin, offshore California. Chemical Geology 205, 265–289.

Paull, C.K., Fullagar, P.D., Bralower, T.J., Röhl, U., 1995a. Seawater ventilation of Mid-Pacific guyots drilled during Leg 143. In: Winterer, E.L., Sager, W.W., Firth, J.V., Sinton, J.M. (Eds.), Proceedings of the Ocean Drilling Program, Scientific Results. Ocean Drilling Program, College Station, TX, pp. 231–241.

Paull, C.K., Ussler III, W., Borowski, W.S., Spiess, F.N., 1995b. Methane-rich plumes on the Carolina continental rise; associations with gas hydrates. Geology 23 (1), 89–92.

Paytan, A., Kastner, M., Martin, E.E., MacDougall, J.D., Herbert, T., 1993. Marine barite as a monitor of seawater strontium isotope composition. Nature 366, 445–449.

Peckmann, J., Reimer, A., Luth, U., Luth, C., Hansen, B.T., Heinicke, C., Hoefs, J., Reitner, J., 2001. Methane-derived carbonates and authigenic pyrite from the northwestern Black Sea. Marine Geology 177 (1–2), 129–150.

Reitner, J., Peckmann, J., Blumenberg, M., Michaelis, W., Reimer, A., Thiel, V., 2005. Concretionary methane-seep carbonates and associated microbial communities in Black Sea sediments. Palaeogeography, Palaeoclimatology, Palaeoecology 227 (1–3), 18–30.

Rosenbaum, J., Sheppard, S.M.F., 1986. An isotopic study of siderites, dolomites and ankerites at high temperatures. Geochimica et Cosmochimica Acta 50, 1147–1150.

Sample, J.C., Reid, M.R., 1998. Contrasting hydrogeologic regimes along strike-slip and thrust faults in the Oregon convergent margin: evidence from the chemistry of syntectonic carbonate cements and veins. Geological Society of America Bulletin 110 (1), 48–59.

Savard, M.M., Beauchamp, B., Veizer, J., 1996. Significance of aragonite cements around Cretaceous marine methane seeps. Journal of Sedimentary Research 66 (3), 430–438.

Stakes, D.S., Orange, D.L., Paduan, J.B., Salamy, K., Maher, N., 1999. Cold-seeps and authigenic carbonate formation in Monterey Bay, California. Marine Geology 159 (1–4), 93–109.

Stakes, D.S., Trehu, A.M., Goffredi, S.K., Naehr, T.H., Duncan, R.A., 2002. Mass wasting, methane venting, and biological communities on the Mendocino transform fault. Geology 30 (5), 407–410.

Suess, E., Carson, B., Ritger, S.D., Moore, J.C., Jones, M.L., Kulm, L.D., Cochrane, G.R., 1985. Biological communities at vent sites along the subduction zone off Oregon. In: Jones, M.L. (Ed.), The Hydrothermal Vents of the Eastern Pacific: an Overview. Bulletin of the Biological Society of Washington. pp. 475–484.

Swart, P.K., Burns, S.J., Leder, J.J., 1991. Fractionation of the stable isotopes of oxygen and carbon in carbon dioxide during the reaction of calcite with phosphoric acid as a function of temperature and technique. Chemical Geology 86, 89–96.

Thiel, V., Peckmann, J., Seifert, R., Wehrung, P., Reitner, J., Michaelis, W., 1999. Highly isotopically depleted isoprenoids: molecular markers for ancient methane venting. Geochimica et Cosmochimica Acta 63 (23/24), 3959–3966.

Vernon, J.W., Slater, R.A., 1963. Submarine tar mounds, Santa Barbara County, California. Bulletin of the American Association of Petroleum Geologists 47 (8), 1624–1627.

Whiticar, M.J., 1999. Carbon and hydrogen isotope systematics of bacterial formation and oxidation of methane. Chemical Geology 161, 291–314.

Wilkinson, E.R., 1971. California offshore oil and gas seeps. Annual Report of the State Oil and Gas Supervisor 57 (1), 5–28.

Winter, B.L., Knauth, L.P., 1992. Stable isotope geochemistry of carbonate fracture fills in the Monterey Formation, California. Journal of Sedimentary Petrology 62, 208–219.